Cluster percolation in the three-dimensional $\pm J$ random-bond Ising model

L. Münster[1] and M. Weigel[1,2]
[1]*Institut für Physik, Technische Universität Chemnitz, 09107 Chemnitz, Germany*
[2]*Physics Department, Emory University, Atlanta, Georgia, USA*

(Received 13 November 2025; accepted 2 February 2026; published 26 February 2026)

Based on extensive parallel-tempering Monte Carlo simulations, we investigate the relationship between cluster percolation and equilibrium ordering phenomena in the three-dimensional $\pm J$ random-bond Ising model for different fractions of antiferromagnetic bonds. We consider a range of cluster definitions, most of which are constructed in the space of overlaps between two independent replicas of the system. In the pure ferromagnet that is contained as a limiting case in the class of problems considered, the relevant percolation point coincides with the thermodynamic ordering transition. For the disordered ferromagnet encountered first on introducing antiferromagnetic bonds and the adjacent spin-glass phase of strong disorder, this connection is altered, and one finds a percolation transition above the thermodynamic ordering point that is accompanied by the appearance of *two* percolating clusters of equal density. Only at the lower (disordered) ferromagnetic or spin-glass transition points the densities of these two clusters start to diverge, thus providing a percolation signature of these thermodynamic transitions. We compare the scaling behavior at this secondary percolation transition with the thermodynamic behavior at the corresponding ferromagnetic and spin-glass phase transitions.

DOI: 10.1103/y464-wxbk

I. INTRODUCTION

Cluster-based approaches provide elegant and versatile descriptions of the phenomena at continuous thermodynamic phase transitions [1–3]. While the list of applications of such approaches is long, and new systems with geometric descriptions keep being added (see, e.g., Ref. [4]), this is particularly true for unfrustrated lattice spin models [3,5]. A prototypical example is the usage of Fortuin–Kasteleyn–Coniglio–Klein (FKCK) clusters in the Ising ferromagnet [6,7]. The construction of these clusters allows for a mapping between the paramagnetic–ferromagnetic phase transition and the percolation transition of FKCK clusters, where the density of the largest cluster is equal to the magnetization. Furthermore, the corresponding Swendsen–Wang cluster Monte Carlo dynamics [8,9], which is based on FKCK clusters, drastically reduces the effect of critical slowing down in comparison to local algorithms and thus provides a powerful tool for simulations [10,11].

For frustrated systems such as spin glasses [12–15], a similarly close connection between the percolation of spin clusters and the thermal phase transition has not, in general, been established. In fact, it has been shown that in such systems spin clusters and even FKCK clusters percolate at high temperatures far above the ordering transition [16–20]. While in the pure ferromagnet and even in unfrustrated disordered magnets, the spin-spin correlation function follows from the probability $\gamma_{\boldsymbol{xy}}$ for spins at $\boldsymbol{x}$ and $\boldsymbol{y}$ to be in the same cluster,

$$|\langle s_{\boldsymbol{x}} s_{\boldsymbol{y}}\rangle_S| = \langle \gamma_{\boldsymbol{xy}}\rangle_{\mathrm{cl}}, \tag{1}$$

in the presence of frustration, this identity is weakened to an inequality, viz.

$$|\langle s_{\boldsymbol{x}} s_{\boldsymbol{y}}\rangle_S| \leqslant \langle \gamma_{\boldsymbol{xy}}\rangle_{\mathrm{cl}}. \tag{2}$$

Consequently, the direct relation between the density of the largest cluster and the order parameter in the ferromagnet is lost for the case of frustrated systems, where FKCK cluster percolation no longer implies the presence of long-range order [21] (but see Ref. [22] for a possible generalization). For spin glasses, long-range ferromagnetic order is absent and, instead, there is spin-glass ordering evidenced by the appearance of a nonzero overlap between two independent replicas [12]. It is hence natural to consider cluster definitions derived from multiple replicas [20,23–25] to describe such transitions. Chayes, Machta, and Redner [26] as well as Jörg [27] (CMRJ) have provided a cluster definition in this spirit.

CMRJ clusters have been studied in the Sherrington–Kirkpatrick (SK) model [28], representing the mean-field limit of spin glasses, where it was shown that the density difference of the two largest clusters is equal to the overlap, becoming nonzero at the spin-glass transition [29,30]. In two dimensions, on the other hand, CMRJ clusters asymptotically do not percolate at non-zero temperature, in agreement with the zero-temperature spin-glass transition there [20]. These CMRJ clusters, as well as a related cluster definition due to Houdayer [31], have also found numerous numerical applications in Monte Carlo simulations [23,31–39].

In the present work, we explore the behavior of different cluster types for the crucial case of three dimensions, where a finite-temperature spin-glass phase is present. To arrive at a fuller picture, we consider the general case of the $\pm J$

random-bond Ising model with different fractions of antiferromagnetic bonds, $0 \leqslant \phi \leqslant 0.5$. Specifically, the model is examined in detail for $\phi = 0$, representing a pure ferromagnet; $\phi = 0.125$, corresponding to a disordered and frustrated ferromagnet; and $\phi = 0.5$, which describes a spin glass. This approach provides insight into the relationship between thermal phase transitions and cluster percolation at different levels of frustration and disorder. Using extensive Markov chain Monte Carlo simulations together with suitable finite-size scaling (FSS) analyses, we study percolation properties of the considered cluster types. In particular, we are focused on the question of when percolating clusters first appear and when density differences between percolating clusters set in. We find that these events coincide with the occurrence of the relevant ordering transitions and, where appropriate, we consider the relation of the corresponding percolation critical exponents to the exponents of the associated thermal transitions.

The rest of this paper is organized as follows: In Sec. II, we introduce the $\pm J$ random-bond Ising model and the associated phase diagram. We then move on to discuss the relevant cluster definitions and some of their basic properties. Section III provides a summary of the considered observables together with the expected FSS behavior. The following three sections present our results for the cases of the pure ferromagnet (Sec. IV), which we studied as a reference, the intermediate case of the disordered and frustrated ferromagnet (Sec. V), and the spin-glass problem with equal proportions of ferromagnetic and antiferromagnetic bonds (Sec. VI). Finally, Sec. VII contains our conclusions and outlook.

II. MODEL, PHASE DIAGRAM, AND CLUSTER DEFINITIONS

We study the $\pm J$ random-bond Ising model with Hamiltonian

$$\widehat{H}_{\boldsymbol{J}}(\boldsymbol{S}) = -\sum_{\langle \boldsymbol{x},\boldsymbol{y}\rangle} J_{\boldsymbol{xy}} s_{\boldsymbol{x}} s_{\boldsymbol{y}}. \tag{3}$$

The Ising spins $s_{\boldsymbol{x}} \in \{\pm 1\}$ are placed on the sites of a cubic lattice of linear size L such that there are $N = L^3$ spins in total. The symbol $\langle \boldsymbol{x}, \boldsymbol{y}\rangle$ refers to the summation over nearest neighbors only. In our actual calculations, we always take periodic boundary conditions to remove surface effects. The exchange couplings $J_{\boldsymbol{xy}}$ are time-independent (quenched) random variables which, for the purposes of the present work, are drawn from a bimodal distribution,

$$P_J(J_{\boldsymbol{xy}}) = \phi\, \delta(J_{\boldsymbol{xy}} + 1) + (1 - \phi)\, \delta(J_{\boldsymbol{xy}} - 1), \tag{4}$$

that is, a bond is either antiferromagnetic $J_{\boldsymbol{xy}} = -1$ with probability ϕ or ferromagnetic $J_{\boldsymbol{xy}} = 1$ with probability $1 - \phi$. The bond is said to be satisfied if $J_{\boldsymbol{xy}} s_{\boldsymbol{x}} s_{\boldsymbol{y}} = 1$ and broken if $J_{\boldsymbol{xy}} s_{\boldsymbol{x}} s_{\boldsymbol{y}} = -1$. A key property of this Hamiltonian is the presence of frustration for any $\phi > 0$. A system is said to be frustrated if no spin configuration exists that satisfies all bonds simultaneously.

The model is studied in the canonical ensemble at temperature T such that, in equilibrium, the spin configurations $\boldsymbol{S} \in \{\pm 1\}^N$ are Gibbs–Boltzmann distributed. The properties of the thermodynamic state of the model are determined by two parameters: the temperature T and the fraction of antiferromagnetic bonds ϕ. Depending on these parameters, the system is in one of four distinct phases. At high temperatures, the system is in a paramagnetic phase, while at low temperatures it transitions either into a ferromagnetic or antiferromagnetic phase, or into the spin-glass phase, depending on the value of ϕ. Since for the bipartite simple cubic lattice the antiferromagnetic phase is simply related by symmetry to the ferromagnetic one, we restrict our attention to the regime $0 \leqslant \phi \leqslant 1/2$. To differentiate between the paramagnetic, ferromagnetic, and spin-glass phases, two order parameters are introduced: the magnetization, which characterizes the ferromagnetic state, and the overlap, which describes the spin-glass state. The magnetization of a single spin configuration is given by

$$\widehat{m}(\boldsymbol{S}) = \frac{1}{N} \sum_{\boldsymbol{x}} s_{\boldsymbol{x}}. \tag{5}$$

Within the ferromagnetic phase, the average magnetization $m := [\langle |\widehat{m}| \rangle_S]_J$ is nonzero, whereas in the paramagnetic and spin-glass phases it approaches zero in the thermodynamic limit. Here, $\langle \cdots \rangle_S$ represents the thermal average taken over the Gibbs–Boltzmann distribution, while $[\cdots]_J$ denotes the average over the quenched disorder. The overlap is the order parameter of the spin-glass transition and is defined by

$$\widehat{q}(\boldsymbol{S}^{(1)}, \boldsymbol{S}^{(2)}) = \frac{1}{N} \sum_{\boldsymbol{x}} q_{\boldsymbol{x}}, \tag{6}$$

where $q_{\boldsymbol{x}} = s_{\boldsymbol{x}}^{(1)} s_{\boldsymbol{x}}^{(2)}$ and $s_{\boldsymbol{x}}^{(1)} \in \boldsymbol{S}^{(1)}$, $s_{\boldsymbol{x}}^{(2)} \in \boldsymbol{S}^{(2)}$. Here $\boldsymbol{S}^{(1)}$ and $\boldsymbol{S}^{(2)}$ denote two spin configurations that belong to different, independent replicas of the system. Accordingly, the average overlap $q := [\langle |\widehat{q}| \rangle_{S_2}]_J$ is computed using the two-replica Gibbs–Boltzmann distribution,

$$P_{S_2}(\boldsymbol{S}^{(1)}, \boldsymbol{S}^{(2)} | \boldsymbol{J}) = \frac{1}{Z_{\boldsymbol{J}}^2} \exp\left(-\widehat{H}_{\boldsymbol{J}}^{(2)}/T\right) \text{ with}$$
$$\widehat{H}_{\boldsymbol{J}}^{(2)} = -\sum_{\langle \boldsymbol{x},\boldsymbol{y}\rangle} J_{\boldsymbol{xy}} \tilde{s}_{\boldsymbol{x}} \tilde{s}_{\boldsymbol{y}}. \tag{7}$$

Here, $\tilde{s}_{\boldsymbol{x}} = (s_{\boldsymbol{x}}^{(1)}, s_{\boldsymbol{x}}^{(2)})$ are two-component vector spins such that $\tilde{s}_{\boldsymbol{x}} \tilde{s}_{\boldsymbol{y}} = s_{\boldsymbol{x}}^{(1)} s_{\boldsymbol{y}}^{(1)} + s_{\boldsymbol{x}}^{(2)} s_{\boldsymbol{y}}^{(2)}$, and $Z_{\boldsymbol{J}}$ is the partition function for a given realization $\boldsymbol{J}$ of bonds. Note that, for convenience, the Boltzmann constant is set to $k_{\mathrm{B}} := 1$. Asymptotically, the overlap is nonzero in the ferromagnetic and in the spin-glass phase, whereas it is zero in the paramagnetic phase.

In Fig. 1, we show a schematic phase diagram of the three-dimensional $\pm J$ random-bond Ising model [40], based on data from Refs. [19,41–45]. The boundary separating the paramagnetic and ferromagnetic phases starts at the Ising critical point [46] $T_{\mathrm{I}} := T_{\mathrm{f}}(0) = 4.511\,523\,26(11)$, which falls within the Ising universality class. The boundary then extends downward to the multicritical point [43] at $T^* = 1.6692(3)$ and $\phi^* = 0.231\,80(4)$. In the interval $0 < \phi < \phi^*$, the paramagnetic–ferromagnetic phase transition belongs to the disordered Ising universality class [41]. At the multicritical point, also referred to as the Nishimori point, the paramagnetic, spin-glass, and ferromagnetic phases meet. Beyond this point, where $\phi^* < \phi \leqslant 0.5$, the phase transition between the paramagnetic and spin-glass phases belongs to the Ising spin-glass universality

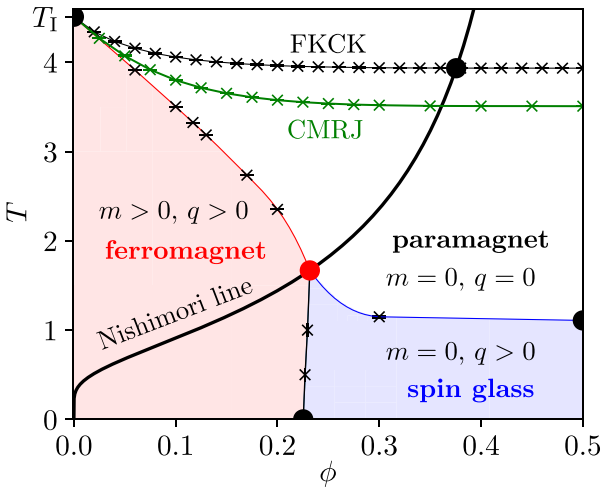

FIG. 1. Phase diagram of the three-dimensional $\pm J$ random-bond Ising model according to the data of Refs. [19,41–45]. The data points for the CMRJ percolation transition originate from the present study (green crosses). The red dot illustrates the location of the multicritical Nishimori point. The black dots indicate important transition points: the pure Ising critical point, the intersection of the FKCK transition line with the Nishimori line, the spin-glass transition temperature for $\phi = 0.5$, and the zero-temperature transition between the ferromagnetic and spin-glass phases. The lines connecting the data points are included as visual guides, except for the Nishimori line, which is explicitly defined in Eq. (11).

class [42,47,48]. At the endpoint of the transition line, where half of the bonds are antiferromagnetic, the spin-glass transition temperature is [48] $T_{\rm sg}(0.5) = 1.1019(29)$. The boundary between the ferromagnetic and spin-glass phases extends from [45] $T_{\rm f}(\phi_0) = 0$ at $\phi_0 = 0.2253(7)$ up to the multicritical point [44,49]. The phase diagram can be symmetrically extended to values of $0.5 < \phi \leqslant 1$. In this case, the magnetization needs to be replaced by the staggered magnetization in order to identify antiferromagnetic order instead of ferromagnetic order.

The aim of the present study is to characterize thermal phase transitions in the $\pm J$ random-bond Ising model through the properties of several types of clusters. The corresponding bond-percolation problem is introduced as follows: each bond in the system is occupied with a probability p_{xy}, and clusters are formed based on the occupied bonds. Specifically, all spin sites that can be connected through a path of occupied bonds belong to the same cluster. The smallest possible cluster consists of just one spin site, while the largest can contain all the sites. The tuning parameter of percolation is the occupation probability. In the percolation problems discussed here, the occupation probability depends on the underlying spin configurations. This contrasts with random percolation, where each bond is occupied independently with a uniform probability [3]. Typically, there is a nonpercolating subcritical phase for low occupation probabilities and a percolating supercritical phase for high occupation probabilities. The system is said to percolate if there is one or more clusters that span the entire system. The percolation threshold $p_{\rm th}$ denotes the critical occupation probability above which an infinite (percolating) cluster exists in the thermodynamic limit.

A straightforward way to define meaningful clusters in the Ising model is by identifying regions where the order parameter takes an identical value [3]. For the magnetization, bonds are hence activated between all like spins, and the bond-occupation probability is thus given by

$$p_{xy}^{(\rm Ising)} = \begin{cases} 1 & \text{if } s_x = s_y \\ 0 & \text{else,} \end{cases} \tag{8}$$

and we denote the corresponding clusters as Ising clusters. In the same spirit, given two replicas, geometric clusters can be defined in the domains of constant overlap. In this case, the bond occupation probability is given by

$$p_{xy}^{(\rm H)} = \begin{cases} 1 & \text{if } q_x = q_y \\ 0 & \text{else,} \end{cases} \tag{9}$$

and we denote the corresponding clusters as Houdayer clusters [31]. Although both Ising and Houdayer clusters are useful to describe the phases of the $\pm J$ random-bond Ising model, they do not properly represent the correlations of the order parameters. Clusters that have this property, at least when the system is not frustrated, are the single-replica FKCK clusters with bond-occupation probability [6,7]

$$p_{xy}^{(\rm FKCK)} = \begin{cases} 1 - \exp\left(-\dfrac{2J_{xy}s_x s_y}{T}\right) & \text{if } J_{xy}s_x s_y > 0 \\ 0 & \text{else.} \end{cases} \tag{10}$$

For the pure Ising model at $\phi = 0$, the FKCK percolation transition maps onto the ferromagnetic phase transition, see Eq. (1), exhibiting identical critical behavior [3]. However, for $\phi > 0$, this mapping breaks down, cf. Eq. (2), and the critical temperature of the percolation transition exceeds that of both the ferromagnetic and spin-glass transitions [17,18,21]. According to Monte Carlo simulations, the FKCK percolation transition for values of $\phi > 0$ belongs to the universality class of random percolation [16,19]. On the Nishimori line, the critical temperature of the FKCK percolation transition can be determined using the random-bond percolation threshold of the cubic lattice, given by [50] $p_{\rm th} = 0.248\,811\,82(10)$. The Nishimori line is a special set in parameter space derived via a gauge transformation. On this line, physical quantities such as the internal energy can be computed exactly, and remarkable correlation identities hold [51,52]. The line originates at $T = 0$ for $\phi = 0$, passes through the multicritical point, and diverges as $\phi \to 0.5$. Its precise form is defined by [52]

$$T_{\rm N}(\phi) = \frac{2}{\ln\left[(1-\phi)/\phi\right]}. \tag{11}$$

At $\phi_{\text{N-FKCK}} = (1 - p_{\rm th})/2$ the Nishimori line intersects the FKCK transition line [53–55] as shown in Fig. 1. At this intersection, it has been rigorously proven that the FKCK transition belongs to the random-percolation universality class [55].

For $\phi > 0$, the physical interpretation of the FKCK percolation transition remains unclear [55–57]. Instead, a more meaningful approach is to consider clusters defined across multiple replicas that can be directly linked to the overlap [23], such as Houdayer clusters. A two-replica cluster definition, in this spirit, emerges from the graphical representation of Chayes, Machta, and Redner [26,29,30], as well as from

the cluster algorithm of Jörg [27]. The bond-occupation probability of these CMRJ clusters is given by [58]

$$p_{xy}^{(\mathrm{CMRJ})} = \begin{cases} 1 - \exp\left(-\dfrac{2J_{xy}\tilde{s}_x\tilde{s}_y}{T}\right) & \text{if } J_{xy}\tilde{s}_x\tilde{s}_y > 0 \\ 0 & \text{else.} \end{cases} \tag{12}$$

This implies that a bond is occupied only if it is simultaneously satisfied in both replicas. Consequently, spins within the same CMRJ cluster share an identical value of the overlap. The results for the percolation temperatures of the CMRJ clusters, presented in Fig. 1, indicate that these clusters percolate within the temperature range between the FKCK percolation transition and the thermal phase transition for $0 < \phi \leqslant 0.5$. In the special case of $\phi = 0$, CMRJ clusters percolate precisely at the critical temperature of the pure ferromagnet, T_{I}.

Note that Newman and Stein also proposed a definition for multireplica clusters in spin glasses, the two-replica FKCK clusters [57]. These ideas are further discussed in Appendix D.

III. OBSERVABLES AND FINITE-SIZE SCALING

To investigate the connection between the thermal (ferromagnetic or spin-glass) phase transitions in the disordered Ising model and the percolation transitions of the various types of clusters considered, we study observables that are able to describe magnetic and spin-glass ordering as well as quantities typically considered in percolation theory.

A. Percolation quantities

Clusters naturally are the central objects of interest in percolation [59–61]. The density $\widehat{\rho}$ of a cluster is defined as the number of sites contained in the cluster, also referred to as the cluster size, divided by the total number N of lattice sites in the system. In the following, we assume that the clusters are ordered by their densities such that $\widehat{\rho}_i \geqslant \widehat{\rho}_{i+1}$ for $i = 1, 2, 3, \ldots$, meaning that $\widehat{\rho}_1$ represents the largest cluster, $\widehat{\rho}_2$ the second largest, and so forth. The order parameter of the percolation transition is the density of the largest cluster, $\rho_1 = [\langle\widehat{\rho}_1\rangle_{\mathrm{cl}}]_J$, also known as the percolation strength P_∞, where $\langle\cdots\rangle_{\mathrm{cl}}$ denotes the average over the configurations of occupied bonds [59].

The tuning parameter of the percolation transition is the occupation probability. For the clusters defined in Sec. II, the occupation probabilities explicitly or implicitly depend on temperature. As a result, the observables are studied as functions of temperature. According to finite-size scaling, the leading-order singular behavior of the largest cluster in the critical region is given by [59]

$$L^{\beta/\nu}\rho_1 = \Psi_\rho(tL^{1/\nu}), \tag{13}$$

where $t = (T - T_{\mathrm{c}})/T_{\mathrm{c}}$ is the reduced temperature and Ψ_ρ is the corresponding scaling function. Here T_{c} denotes the critical temperature of the percolation transition of the considered clusters, which is analogous to the percolation threshold in random percolation. At the critical temperature, the average cluster size diverges as [59]

$$\chi_\rho(T_{\mathrm{c}}) \sim L^{\gamma/\nu}, \tag{14}$$

where

$$\chi_\rho = N\left[\left\langle\sum_{i=1}\widehat{\rho}_i^2\right\rangle_{\mathrm{cl}}\right]_J.$$

The sum runs over the densities of all clusters. The percolation transition separates the high-temperature phase, characterized by local clusters only, from the percolating phase, where there is at least one system-spanning cluster. In this work, only finite-size systems with periodic boundary conditions in all directions are considered, and the criterion for percolation is satisfied if a cluster wraps around the boundaries in at least one direction. The wrapping probability, thus, provides information about the location of the percolation transition [62]. The wrapping probability is a dimensionless quantity that follows the scaling form [59]

$$R(t, L) = \Psi_R(tL^{1/\nu}). \tag{15}$$

If there is more than one wrapping cluster, the number of wrapping clusters w_R can also be studied as an observable. The number of wrapping clusters obeys the same scaling law as the wrapping probability.

B. Thermal quantities

To establish a connection between geometric and thermal properties, it is necessary to investigate the behavior of the thermal order parameters m and q. To leading order, m and q satisfy the scaling laws [63]

$$L^{\beta/\nu}m = \Psi_m(tL^{1/\nu}) \quad \text{or} \quad L^{\beta/\nu}q = \Psi_q(tL^{1/\nu}), \tag{16}$$

in the critical region of the respective phase transition. Specifically, this corresponds to a ferromagnetic transition in the case of the magnetization and to a spin-glass transition in the case of the overlap. At the critical point, the susceptibility diverges as [63]

$$\chi_{m/q}(T_{\mathrm{c}}) \sim L^{\gamma/\nu}, \tag{17}$$

where $\chi_m = N[\langle\widehat{m}^2\rangle_S]_J$ or $\chi_q = N[\langle\widehat{q}^2\rangle_{S_2}]_J$, depending on the transition. Furthermore, in the critical region, the correlation length $\xi_{m/q}$ behaves as [64]

$$\frac{\xi_{m/q}(t, L)}{L} = \Psi_{\xi_{m/q}}(tL^{1/\nu}). \tag{18}$$

The correlation length is here computed using the second-moment estimator, which is based on the Fourier transform $\widetilde{g}_{m/q}(\boldsymbol{k})$ of the two-point correlation function $g_{m/q}(\boldsymbol{r})$, i.e., [63]

$$\xi_{m/q} = \frac{1}{2\sin(k_{\min}/2)}\sqrt{\frac{\widetilde{g}_{m/q}(\boldsymbol{0}) - \widetilde{g}_{m/q}(\boldsymbol{k})}{\widetilde{g}_{m/q}(\boldsymbol{k})}}, \tag{19}$$

where $\boldsymbol{k} = (k_{\min}, 0, 0)$, $k_{\min} = 2\pi/L$, and $\boldsymbol{0} = (0, 0, 0)$. Depending on the context, the correlations of the magnetization, $g_m(\boldsymbol{r}) = [\langle s_{\boldsymbol{0}} s_{\boldsymbol{0}+\boldsymbol{r}}\rangle_S]_J$, or of the overlap, $g_q(\boldsymbol{r}) = [\langle q_{\boldsymbol{0}} q_{\boldsymbol{0}+\boldsymbol{r}}\rangle_{S_2}]_J$, are considered.

C. Simulations and finite-size scaling analysis

The thermal and geometrical properties of the $\pm J$ random-bond Ising model, as characterized by the above sets of corresponding observables, are studied utilizing parallel-tempering

Monte Carlo simulations. To achieve good equilibration, we employ a combination of single-spin flip, parallel tempering, and cluster-update moves. All data are averaged over a large number of disorder realizations in order to bring down statistical errors to an acceptable level. More information regarding the simulation scheme, including details about the system sizes considered and the number of disorder samples employed, is provided in Appendix E.

The numerical strategy for extracting the critical temperature and critical exponents is as follows. In the first step, a data collapse of the wrapping probability or the number of wrapping clusters is carried out in order to determine T_c and ν of a percolation transition, according to Eq. (15). To obtain T_c and ν of a thermal phase transition, a similar data collapse is performed using the correlation length and Eq. (18). In the second step, a power law is fitted to the data of the average cluster size or the susceptibility at the previously estimated value of the critical temperature T_c, yielding γ/ν via Eq. (14) or Eq. (17), respectively. Since a data point at T_c is not necessarily available, a linear interpolation of the relevant quantity is carried out to obtain the value. To extract the critical exponent β/ν, a data collapse of the order parameter is performed according to the scaling law in Eq. (13) or Eq. (16), fixing $1/\nu$ to the previously determined value. The optimal parameters for the data collapses are extracted using the tool provided in Ref. [65]. Our analysis focuses on the behavior of the $\pm J$ random-bond Ising model for three distinct fractions of antiferromagnetic bonds, $\phi = 0$, $\phi = 0.125$, and $\phi = 0.5$. We first focus on the reference case $\phi = 0$.

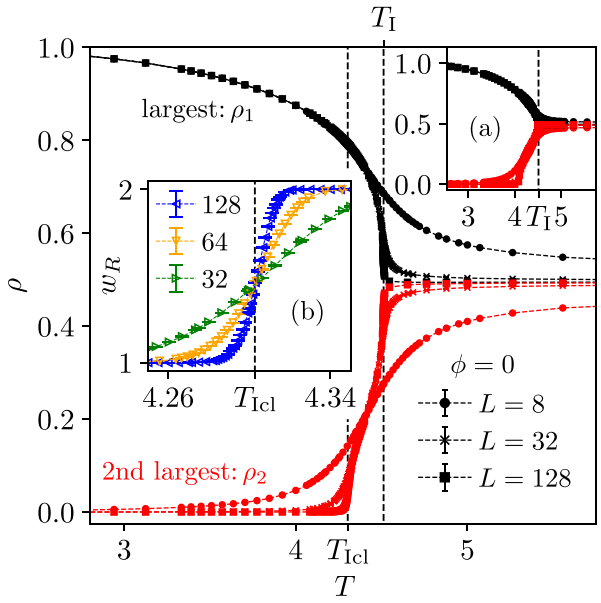

FIG. 2. Densities of the two largest Ising clusters as a function of temperature for the pure ferromagnet using three exemplary system sizes, $L = 8$, $L = 32$, and $L = 128$. Inset (a) shows the corresponding relationship for the Houdayer clusters. T_I denotes the critical temperature of the ferromagnetic phase transition. Inset (b) illustrates how the number of wrapping Ising clusters decreases from two to one at T_{Icl} (see main text for details). The system sizes plotted are $L = 32$, 64, and 128.

IV. CLUSTERS IN THE PURE FERROMAGNET

When $\phi = 0$, there are no antiferromagnetic bonds present, and the Hamiltonian in Eq. (3) reduces to that of a pure, unfrustrated Ising ferromagnet. This model undergoes a phase transition from the paramagnetic to the ferromagnetic phase at [46] $T_I = 4.511\,523\,26(11)$. As illustrated in Fig. 2, this phase transition is visible in both the Ising and Houdayer clusters [66]. The figure shows the behavior of the largest and second-largest cluster as a function of temperature. At high temperatures, there are two giant percolating clusters with equal densities. The reason is that for $T \to \infty$, spin orientations are random, so on average half of the spins are up and the other half down, causing both Houdayer and Ising clusters to behave similarly to a random-site percolation problem. The site-percolation threshold on a cubic lattice is [50] $p_{th}^{(s)} = 0.311\,607\,7(2) < 1/2$. As a result, there are two percolating clusters, one with positive and the other with negative values of the magnetization or overlap, respectively. This argument remains valid for any value of ϕ when $T \to \infty$. At the ferromagnetic phase transition, one cluster begins to dominate the other, and the densities start to deviate from $\rho_{1/2} \approx 0.5$. Figure 2(b) shows how the number of wrapping Ising clusters decreases from two to one at the temperature [67] $T_{Icl} = 4.3027(3)$. Notably, this temperature is lower than the critical temperature of the ferromagnetic phase transition [66]. Hence, Ising clusters clearly do not encapsulate the critical behavior of the thermal phase transition. Somewhat differently, in two dimensions, the second largest cluster does percolate right at T_I, but the corresponding critical exponents nevertheless differ from those of the thermal phase transition [68]. Finally, at zero temperature, the magnetization and the overlap reach unity, implying that there is a single Ising or Houdayer cluster containing all spin sites.

Hence, although both Ising and Houdayer clusters reflect the ordering behavior of the model, their percolation properties do not map onto the ferromagnetic phase transition [66,69,70]. Clusters that do exhibit this property, at least for $\phi = 0$, are the FKCK clusters. For them, the spin–spin correlation function is equivalent to the connectivity function of the corresponding percolation problem, cf. Eq. (1) [3,5]. In other words, the correlation between spins $s_{\boldsymbol{x}}$ and $s_{\boldsymbol{y}}$ is identical to the probability that the lattice sites $\boldsymbol{x}$ and $\boldsymbol{y}$ belong to the same FKCK cluster. In general, the behavior of the FKCK clusters differs significantly from that of the previously discussed Ising and Houdayer clusters. At high temperatures, percolation does not occur because the occupation probability depends on temperature and vanishes for $T \to \infty$. Due to Eq. (1), the critical behavior of the FKCK percolation transition is identical to that of the ferromagnetic phase transition. Below the transition temperature, there is a unique largest cluster whose density equals the magnetization in the thermodynamic limit [3].

Interestingly, we observe that for the case of $\phi = 0$ the two-replica CMRJ clusters exhibit the same percolation behavior as the FKCK clusters. Figure 3 illustrates the finite-size scaling behavior of the wrapping probability of CMRJ clusters. From the data collapse, the critical temperature $T_{CMRJ} = 4.511\,527(16)$ and the critical exponent $\nu = 0.6300(17)$ are obtained.

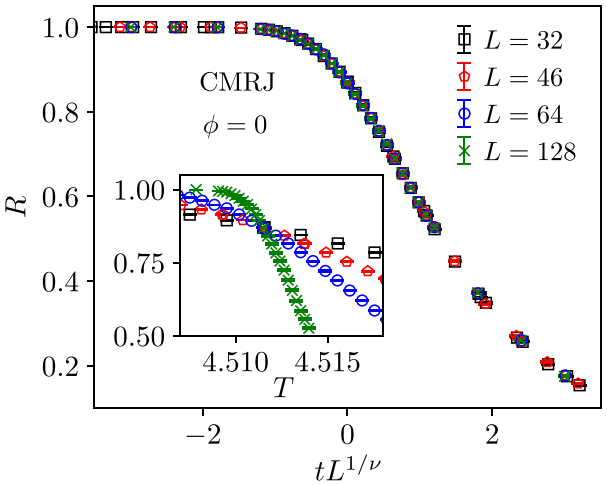

FIG. 3. Data collapse of the wrapping probability of CMRJ clusters, obtained according to Eq. (15), in the critical region of the CMRJ percolation transition for the pure Ising ferromagnet ($\phi = 0$), with $t = (T - T_{\mathrm{CMRJ}})/T_{\mathrm{CMRJ}}$. From this collapse, the critical parameters are estimated as $T_{\mathrm{CMRJ}} = 4.511\,527(16)$ and $\nu = 0.6300(17)$. The inset shows the unscaled data in the vicinity of the critical point.

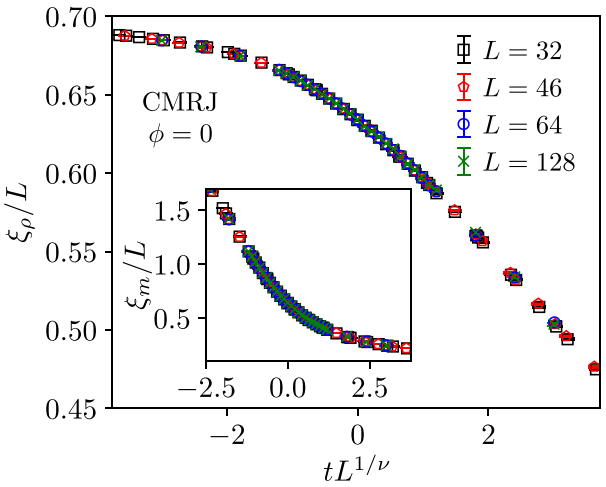

FIG. 4. Data collapse of the connectivity length according to Eq. (22) with $t = (T - T_{\mathrm{CMRJ}})/T_{\mathrm{CMRJ}}$ for the parameters $T_{\mathrm{CMRJ}} = 4.511\,527$ and $\nu = 0.6300$. The inset shows the corresponding data collapse for the correlation length of the order parameter, defined in Eq. (19), using the same parameters, i.e., $T_{\mathrm{I}} = 4.511\,527$, $\nu = 0.6300$, and $t = (T - T_{\mathrm{I}})/T_{\mathrm{I}}$.

To determine the exponent γ/ν, power-law fits are performed using Eq. (14) for the average cluster size at the temperature [46] $T = 4.511\,523\,256$. For small system sizes, we notice the presence of scaling corrections for this quantity, and it is necessary to take these into account in the fits. In the present context, we achieve this by performing a power-extrapolation of effective critical exponents (local slopes) found from fits on a restricted range of system sizes. The detailed procedure is described in Appendix B, where we also include a plot showing the scaling of the average cluster size at the critical temperature. The resulting estimate for the average cluster-size (susceptibility) exponent for the CMRJ clusters is $\gamma/\nu = 1.9638(18)$.

To directly test whether the correlations of the ferromagnetic phase transition and the CMRJ percolation transition behave identically in the vicinity of the phase transition, the critical behavior of the correlation length is compared with that of the cluster connectivity length. The connectivity length can be computed as [59]

$$\xi_\rho = \sqrt{\frac{2N\left[\left\langle \sum_{i=1} \widehat{r}_i^2 \widehat{\rho}_i^2 \right\rangle_{\mathrm{cl}}\right]_J}{\chi_\rho}}. \tag{20}$$

Here, $\widehat{r}_i$ denotes the radius of the ith largest cluster. The radius of a cluster containing n lattice sites is given by [59]

$$\widehat{r} = \sqrt{\frac{1}{n}\sum_{j=1}^{n} |\boldsymbol{r}_j - \boldsymbol{r}_0|^2}. \tag{21}$$

The summation is performed over the Euclidean distances between the positions of the lattice sites in the cluster $\boldsymbol{r}_j$ and the center of mass of the cluster $\boldsymbol{r}_0$. For nonwrapping clusters, the center of mass can be defined with respect to any lattice position. For wrapping clusters, an algorithm proposed in Ref. [71] is used to determine the center of mass. Analogous to the correlation length, the connectivity length follows the scaling form [59]

$$\frac{\xi_\rho(t, L)}{L} = f_{\xi_\rho}(tL^{1/\nu}). \tag{22}$$

Figure 4 shows the data collapses of the connectivity length of the CMRJ clusters and the correlation length of the order parameter, using Eqs. (18) and (22), respectively. The collapse parameters were previously obtained from the wrapping probability of the CMRJ clusters, see Fig. 3. Figure 4 therefore directly demonstrates that the connectivity length and the correlation length exhibit identical critical behavior.

As mentioned above, the density of the largest FKCK cluster equals the magnetization in the thermodynamic limit [3,72]. In other words,

$$\rho_1 = m \tag{23}$$

for $L \to \infty$. This property also holds for the CMRJ clusters, as illustrated in Fig. 5. The inset of this figure shows four different quantities that exhibit the same behavior as functions of temperature and can serve as order parameters of the ferromagnetic phase transition. Notably, the density of the second-largest CMRJ cluster vanishes for $L \to \infty$, so that $\rho_1 - \rho_2 = \rho_1$. Figure 5 also shows that, up to corrections,

$$m = \sqrt{q}$$

in the ordered phase. This identity follows from taking a pure-state average of a spin $s_{\mathbf{x}}$ for the case of translational invariant systems (recall that we are using periodic boundary conditions). In the high-temperature limit $T \to \infty$, in contrast, one sees that $m = q = 1/\sqrt{N}$. From the data collapses of the largest CMRJ cluster shown in the main plot of Fig. 5, the critical exponent $\beta/\nu = 0.516(4)$ is estimated. Note that in this case only the critical temperature and the exponent β/ν are optimized, while the exponent $1/\nu$ is fixed to the previously determined value. This choice is made because the

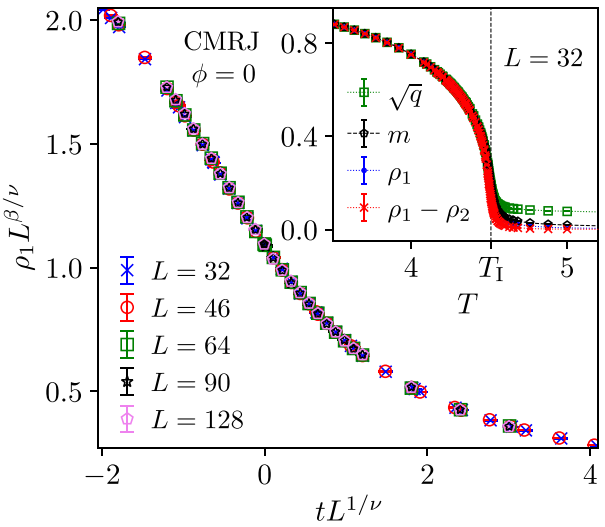

FIG. 5. Data collapse of the density of the largest CMRJ cluster according to Eq. (13) for the pure Ising ferromagnet with $t = (T - T_{\mathrm{CMRJ}})/T_{\mathrm{CMRJ}}$. From this collapse, the values $T_{\mathrm{CMRJ}} = 4.511\,534(26)$ and $\beta/\nu = 0.516(4)$ are obtained. The parameter $1/\nu$, with $\nu = 0.6300$, is held constant during the optimization. The inset illustrates four different quantities, all of which can serve as order parameters of the ferromagnetic phase transition.

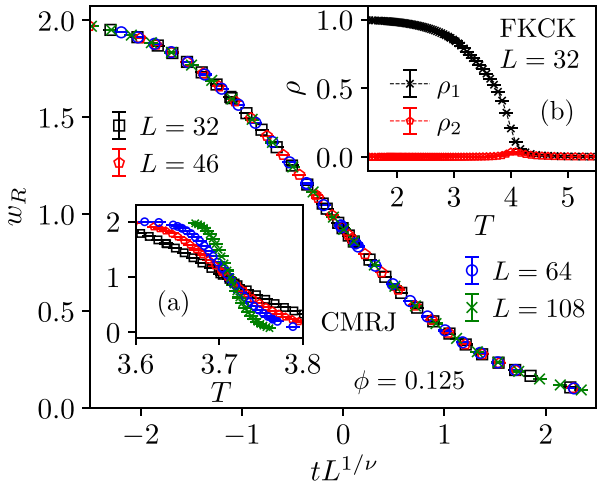

FIG. 6. The main plot shows the number of wrapping CMRJ clusters for $\phi = 0.125$, rescaled according to the scaling law of Eq. (15) with $t = (T - T_{\mathrm{CMRJ}})/T_{\mathrm{CMRJ}}$. The critical quantities are estimated as $T_{\mathrm{CRMJ}} = 3.71523(24)$ and $\nu = 0.875(9)$. Inset (a) illustrates the unscaled data. Inset (b) shows the two largest FKCK clusters for $\phi = 0.125$ at system size $L = 32$. Notably, there is only one wrapping FKCK cluster.

optimization method is more stable if only two parameters are varied [65].

In summary, the estimates collected in Table I indicate that the CMRJ percolation transition belongs to the three-dimensional Ising universality class. This suggests that in the case of a pure Ising ferromagnet, the CMRJ clusters exhibit the same percolation properties as the FKCK clusters. The reason for this is that the correlation function of the two-replica ferromagnet with Hamiltonian

$$\widehat{H}_{\mathrm{I}}^{(2)} = -\sum_{\langle x,y\rangle} \tilde{s}_x \tilde{s}_y \tag{24}$$

is proportional to that of a single ferromagnet at the same temperature [73,74]. Furthermore, the CMRJ clusters can be intuitively interpreted as a two-replica generalization of the FKCK clusters, adapted to the Hamiltonian $\widehat{H}_{\mathrm{I}}^{(2)}$, see Eqs. (10) and (12). As a result, the CMRJ percolation transition maps onto the ferromagnetic phase transition. A more detailed derivation of this result can be found in Appendix A.

TABLE I. Critical quantities of the pure Ising ferromagnet obtained from the correlation length and the susceptibility of the magnetization, as well as the average cluster size and the wrapping probability of the FKCK and CMRJ clusters, respectively. To extract γ/ν we have performed power-law fits at $T = 4.511\,523\,256$ to the data of the susceptibility and the average cluster size according to Eqs. (17) and (14), respectively. The results are in agreement with the more accurate values given in Ref. [46], i.e., $T_c = 4.511\,523\,26(11)$, $\nu = 0.629\,912(86)$, and $\gamma/\nu = 1.963\,90(45)$.

	Magnetization	FKCK	CMRJ
T_c	4.511 537(12)	4.511 522(19)	4.511 527(16)
ν	0.6310(23)	0.630(4)	0.6300(17)
γ/ν	1.965(4)	1.9630(21)	1.9638(18)

V. CLUSTERS IN THE FRUSTRATED DISORDERED FERROMAGNET

The transition between the paramagnetic and ferromagnetic phases for $0 < \phi < \phi^*$ falls within the universality class of the disordered Ising ferromagnet, where [43] $\phi^* = 0.231\,80(4)$ denotes the location of the multicritical point [41]. Due to frustration, the correspondence between the connectivity of FKCK clusters and the spin–spin correlations given in Eq. (1) is no longer valid [21]. As a consequence, for such systems, the connectivity length ξ_ρ is larger than the correlation length $\xi_{m/q}$ [21].

We performed extensive simulations of the system with $\phi = 0.125$. Following the finite-size scaling protocol outlined in Sec. III, we extract an estimate $T_{\mathrm{f}} = 3.2412(4)$ for the ferromagnetic ordering transition. In contrast, the FKCK percolation transition occurs at $T_{\mathrm{FKCK}} = 4.02079(10)$. This transition exhibits the same characteristics as a random percolation transition, with a single infinite cluster in the percolating phase, as shown in Fig. 6(b). The critical exponents of the transition fall within the random percolation universality class [16,19], cf. the data collected in Table II.

As shown in the phase diagram in Fig. 1, the CMRJ percolation transition occurs in the temperature range between the FKCK percolation point and the ferromagnetic phase transition. Unlike the FKCK transition, the CMRJ transition involves the formation of two wrapping clusters, as demonstrated by the data collapse in Fig. 6. The critical temperature is $T_{\mathrm{CMRJ}} = 3.71523(24)$. The CMRJ percolation transition also belongs to the random percolation universality class. Table II summarizes the critical quantities of the three transitions.

TABLE II. Critical quantities of the frustrated disordered ferromagnet for $\phi = 0.125$. The results were obtained by finite-size scaling as described in Sec. III. The ferromagnetic phase transition belongs to the disordered Ising universality class [75]. The FKCK and the CMRJ percolation transitions are part of the random percolation universality class. For comparison, note that, according to Ref. [50], the values for random percolation are $\nu = 0.8764(12)$, $\gamma/\nu = 2.0459(4)$, and $\beta/\nu = 0.47705(15)$.

	Magnetization	FKCK	CMRJ
T_c	3.2412(4)	4.02079(10)	3.71523(24)
ν	0.687(9)	0.873(4)	0.875(6)
γ/ν	1.972(10)	2.0451(24)	2.046(8)
β/ν	0.524(8)	0.475(3)	0.474(8)

The main plot in Fig. 7 illustrates the overlap properties of the largest CMRJ and Houdayer clusters. More precisely, it shows the cluster densities multiplied by the sign of their overlap. The replicas are aligned so that the overlap of the largest cluster is always positive. Let us first focus on Houdayer clusters. In the high-temperature phase, two percolating Houdayer clusters exist, and they exhibit equal density but opposite overlap signs. Consequently, the average overlap is zero. Below the ferromagnetic transition, one cluster dominates the other, and the overlap becomes nonzero. Turning to the CMRJ clusters, their behavior is found to be quite analogous to that of the Houdayer clusters, which is a consequence of CMRJ clusters being geometric subregions of Houdayer clusters. Following Eq. (12), a bond in the CMRJ construction can only be occupied when the overlap at the adjacent lattice sites is identical. Consequently, as $T \to 0$, the two cluster types become essentially indistinguishable. The inset of Fig. 7 shows the general behavior of the number of wrapping CMRJ clusters as a function of temperature. At high temperatures, there is no percolation. At the CMRJ percolation transition, T_{CMRJ}, two percolating clusters emerge. Below the ferromagnetic phase transition, T_f, the number of wrapping CMRJ clusters decreases from two to one.

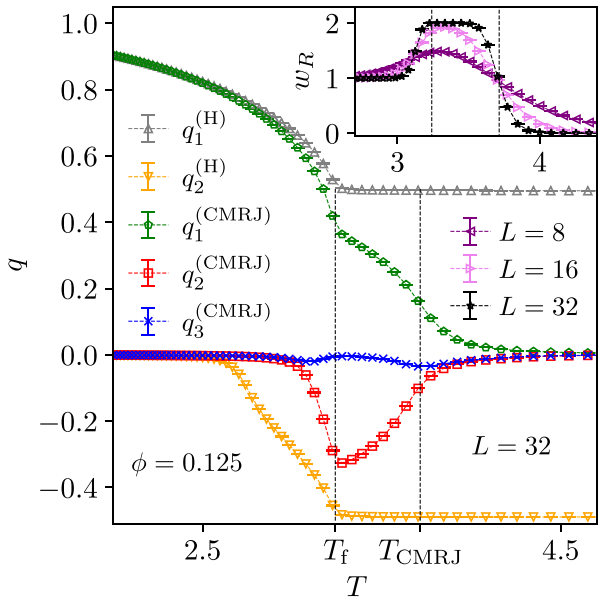

FIG. 7. Relation between the overlap densities of the three largest CMRJ clusters $q_i^{(\mathrm{CMRJ})}$, $i = 1$, 2, and 3, and the two largest Houdayer clusters $q_1^{(\mathrm{H})}$, $q_2^{(\mathrm{H})}$ for $\phi = 0.125$ and $L = 32$. The inset shows the number of wrapping CMRJ clusters for three different system sizes. At T_{CMRJ} two wrapping clusters emerge, see also Fig. 6. Below T_f, the number of wrapping clusters reduces from two to one.

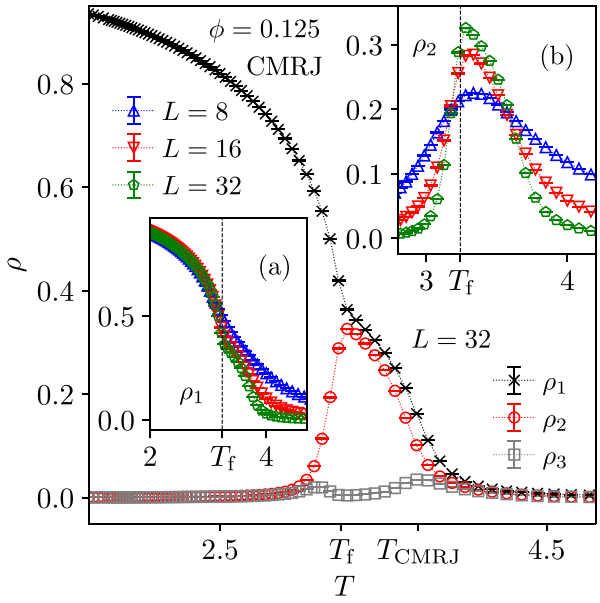

FIG. 8. The densities of the three largest CMRJ clusters as a function of temperature for $\phi = 0.125$ and $L = 32$. Inset (a) shows the behavior of the density ρ_1 of the largest cluster for different system sizes. Inset (b) illustrates how the peak of the second largest cluster increases with system size and how it shifts toward the critical temperature of the ferromagnetic phase transition, T_f.

Figure 8 illustrates the densities of the three largest CMRJ clusters in more detail. In the vicinity of the CMRJ percolation transition, T_{CMRJ}, the third-largest cluster exhibits a peak, which we denote as $\rho_{\mathrm{max}}^{(3)}$. As shown in Fig. 9(a), this peak diminishes with increasing system size. The decay can be approximated by a power law of the form

$$\rho_{\mathrm{max}}^{(3)}(L) = a_{\rho_3} L^{-b_{\rho_3}} + c_{\rho_3}, \tag{25}$$

where the fitted parameters are $a_{\rho_3} = 0.165(4)$, $b_{\rho_3} = 0.426(12)$, and $c_{\rho_3} = -0.0024(8)$. The smallest system size used in the fit is $L_{\mathrm{min}} = 54$, and the quality of the fit is $Q_{\mathrm{fit}} = 0.50$ [76]. This suggests that $\rho_{\mathrm{max}}^{(3)}$ approaches zero in the thermodynamic limit, indicating that, below the CMRJ percolation transition, only the two largest clusters have a nonzero density.

Additionally, the peak in the third-largest cluster size shifts in temperature with increasing system size. This shift is also described by a power law,

$$T_{\mathrm{max}}^{(3)}(L) = a_{T_3} L^{-b_{T_3}} + c_{T_3}. \tag{26}$$

Here, c_{T_3} corresponds to the location of the peak in the thermodynamic limit. The fit, shown in Fig. 9(b), yields $a_{T_3} = 14.8(1.9)$, $b_{T_3} = 2.20(5)$, and $c_{T_3} = 3.71572(26)$ with $L_{\mathrm{min}} = 12$ and $Q_{\mathrm{fit}} = 0.94$. Notably, the value of c_{T_3} is consistent with

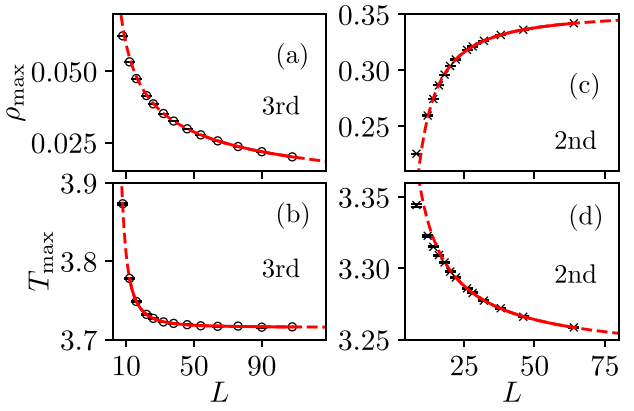

FIG. 9. Behavior of the peak densities of the third and the second largest CMRJ clusters as a function of system size for $\phi = 0.125$. The red lines are power-law fits according to Eqs. (25) and (26), respectively. The dashed red lines are extrapolations of the fits. Panels (a) and (b) show the behavior of the peak of the third largest cluster, and panels (c) and (d) show the same relation for the second largest cluster.

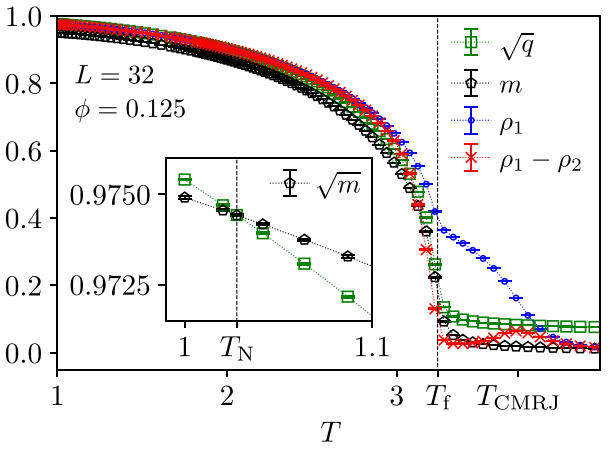

FIG. 10. Relation between the overlap, the magnetization, and the density of the two largest CMRJ clusters for $\phi = 0.125$ and $L = 32$ in the vicinity of the ferromagnetic phase transition. The density difference of the two largest clusters shows a similar behavior as the square root of the overlap, although the quantities are not identical. The inset illustrates that, precisely on the Nishimori line $T_{\rm N}(0.125) = 1.02779\ldots$ the equality $q = m$ is satisfied [52].

the critical temperature of the CMRJ percolation transition, $T_{\rm CMRJ} = 3.71523(24)$.

The peak of the second-largest cluster follows a similar power law as the third-largest cluster, although its density increases with system size, see Fig. 8(b). Figures 9(c) and 9(d) show that the peak shifts toward lower temperatures. Using the same fitting procedure as above, the parameters are determined as $a_{\rho_2} = -2.45(10)$, $b_{\rho_2} = 1.309(14)$, $c_{\rho_2} = 0.35271(23)$ with $L_{\rm min} = 22$ and $Q_{\rm fit} = 0.27$, while the temperature-shift parameters are $a_{T_2} = 0.81(14)$, $b_{T_2} = 0.85(7)$, and $c_{T_2} = 3.235(4)$ with $L_{\rm min} = 22$ and $Q_{\rm fit} = 0.80$. This suggests that, for $L \to \infty$, the peak density of the second-largest cluster is approximately $\rho^{(2)}_{\rm max} = 0.35271(23)$, and that the peak location coincides with the temperature of the ferromagnetic phase transition, since $T^{(2)}_{\rm max} = 3.235(4)$. Note that the shift exponent b_{T_2} does not appear to be compatible with $1/\nu \approx 1.145$ of the thermal transition.

As shown in the inset of Fig. 5, in the ordered phase of the pure ferromagnet, the square root of the overlap approximately equals the density difference of the two largest CMRJ clusters, $\sqrt{q} = \rho_1 - \rho_2$ for $L \to \infty$, where $\rho_2 = 0$ in this case. Although this relation no longer applies for $\phi > 0$, Fig. 10 shows that the density difference of the two largest clusters still qualitatively reproduces the behavior of the magnetization as well as the square root of the overlap.

As a side note, the inset of Fig. 10 illustrates that, on the Nishimori line, the equality $m = q$ is satisfied. This follows from the fact that, on the Nishimori line, the correlations of the magnetization and the overlap coincide [43,52].

VI. CLUSTERS IN THE SPIN-GLASS MODEL

For $\phi = 0.5$, the low-temperature ordered state of the $\pm J$ random-bond Ising model is of spin-glass type. At all temperatures, the system consists of two large Ising clusters with opposite spin orientations, resulting in zero overall magnetization. Furthermore, at high temperatures, there are two large Houdayer clusters with opposite signs of the overlap. As the system undergoes a spin-glass transition, a density difference emerges between these clusters, leading to a nonzero total overlap, as shown in Fig. 11. This transition belongs to the three-dimensional Ising spin-glass universality class [42], with a critical temperature of [48] $T_{\rm sg} = 1.1019(29)$.

A key distinction between this spin-glass transition and the previously discussed ferromagnetic transitions is that the surface of the Houdayer clusters does not exhibit critical behavior. The surface of the Houdayer clusters is connected to the link overlap through the relation

$$\widehat{Q}_{\rm l} = 3N - 2\widehat{Q}_{\rm s}, \tag{27}$$

where $3N$ is the total number of bonds in the system, and $\widehat{Q}_{\rm s}$ is the number of bonds on the surface between regions with positive and negative overlap [77]. The link overlap is

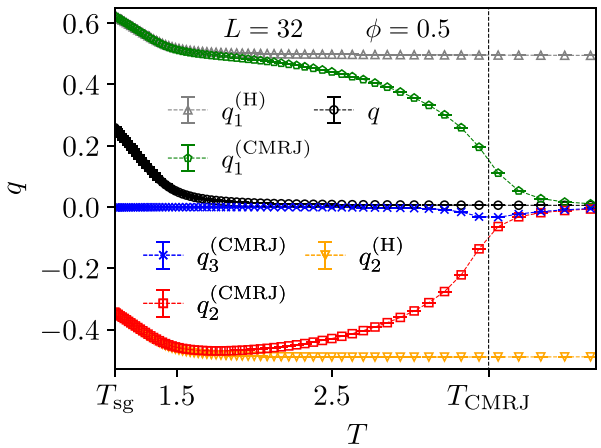

FIG. 11. Overlap densities of the largest Houdayer and CMRJ clusters for $\phi = 0.5$ and system size $L = 32$. At low temperatures, CMRJ clusters are almost indistinguishable from Houdayer clusters.

TABLE III. Critical quantities of the three-dimensional Ising spin glass at $\phi = 0.5$. The values of the spin-glass transition are taken from Ref. [48]. This transition belongs to the Ising spin-glass universality class [42]. The values of the FKCK and CMRJ percolation transitions were obtained by finite-size scaling as described in Sec. III. Both percolation transitions belong to the random percolation universality class.

	Overlap (Ref. [48])	FKCK	CMRJ
T_c	1.1019(29)	3.93410(7)	3.50997(25)
ν	2.562(42)	0.873(4)	0.878(7)
γ/ν	2.39(9)	2.045(3)	2.046(5)
β/ν	0.305(9)	0.474(4)	0.470(6)

defined as

$$\widehat{Q}_\mathrm{l} = \sum_{\langle \boldsymbol{x},\boldsymbol{y}\rangle} s_{\boldsymbol{x}}^{(1)} s_{\boldsymbol{y}}^{(1)} s_{\boldsymbol{x}}^{(2)} s_{\boldsymbol{y}}^{(2)}. \tag{28}$$

In the pure ferromagnet with $\phi = 0$, the link overlap and the energy are related by $q_\mathrm{l} = e_\mathrm{l}^2$, where $q_\mathrm{l} = \langle \widehat{Q}_\mathrm{l}\rangle_{S_2}/(3N)$ and $e_\mathrm{l} = \langle \widehat{H}_\mathrm{l}\rangle_S/(3N)$. Here, $\widehat{H}_\mathrm{l} = -\sum_{\langle \boldsymbol{x},\boldsymbol{y}\rangle} s_{\boldsymbol{x}} s_{\boldsymbol{y}}$ denotes the Hamiltonian of a pure Ising ferromagnet. A similar relationship between the link overlap and the energy also holds for spin glasses with Gaussian couplings, see Refs. [20,78,79]. Consequently, at a ferromagnetic phase transition, the Houdayer cluster surfaces exhibit strong fluctuations, as both the energy and the link overlap are critical quantities. In contrast, at the spin-glass transition, the link overlap and the energy remain nonsingular. Note that the exponent α, which describes the singular part of the specific heat, is negative at the spin-glass transition [48], $\alpha < 0$.

For $\phi = 0.5$, the FKCK percolation transition occurs at $T_\mathrm{FKCK} = 3.93410(7)$ and exhibits the same properties as a random percolation transition with a single infinite cluster. In contrast, the CMRJ clusters percolate at a lower temperature $T_\mathrm{CMRJ} = 3.50997(25)$. Both transitions belong to the random-percolation universality class. The critical quantities for these transitions are listed in Table III. The results were obtained by finite-size scaling, as described in Sec. III. In addition, Table III also includes critical exponents of the Ising spin-glass transition taken from Ref. [48].

Figure 11 illustrates that, at the CMRJ percolation transition, T_CMRJ, two system-spanning clusters of equal density emerge, which are subregions of the two Houdayer clusters. At the spin-glass transition, these two clusters develop a density difference. In Fig. 12, we show the behavior of the three largest CMRJ clusters in more detail. The third-largest cluster exhibits a peak close to the CMRJ percolation transition. To analyze this peak as a function of system size, the fitting approach from Sec. V is applied, using Eqs. (25) and (26). Figures 13(a) and 13(b) show the peak behavior of the density of the third-largest CMRJ cluster. The peak shifts toward the critical temperature of the CMRJ percolation transition, with parameters $a_{T_3} = 7.8(1.1)$, $b_{T_3} = 2.04(5)$, and $c_{T_3} = 3.51022(19)$ for $L_\mathrm{min} = 16$, with $Q_\mathrm{fit} = 0.60$. Furthermore, the peak density $\rho_\mathrm{max}^{(3)}$ decreases to zero as $L \to \infty$, suggesting that there are only two macroscopic clusters below the CMRJ percolation transition. In this case, the fitting

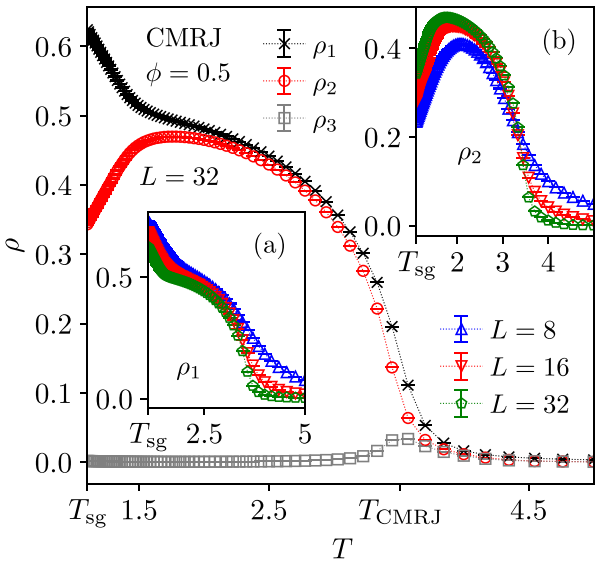

FIG. 12. The density of the three largest CMRJ clusters close to the CMRJ percolation transition for $\phi = 0.5$ and system system size $L = 32$. Insets (a) and (b) display the densities of the largest and second-largest clusters, respectively, for three different system sizes.

parameters are $a_{\rho_3} = 0.1750(18)$, $b_{\rho_3} = 0.451(6)$, and $c_{\rho_3} = -0.0012(4)$ with $L_\mathrm{min} = 38$ and $Q_\mathrm{fit} = 0.44$.

Inset (b) of Fig. 12 depicts how the second-largest CMRJ cluster increases as a function of system size and shifts toward lower temperatures. To study its properties, we again use the fitting procedure according to Eqs. (25) and (26). The results are shown in Figs. 13(c) and 13(d), illustrating how the peak of the second-largest CMRJ cluster shifts toward the spin-glass transition temperature, with fitting parameters $a_{T_2} = 1.783(12)$, $b_{T_2} = 0.299(29)$, and $c_{T_2} = 1.13(7)$ for $L_\mathrm{min} = 12$ and $Q_\mathrm{fit} = 0.47$. The value of the shift exponent b_{T_2} might be compared with the intrinsic shift exponent of the spin-glass transition, $1/\nu \approx 0.39$. At its peak density, the

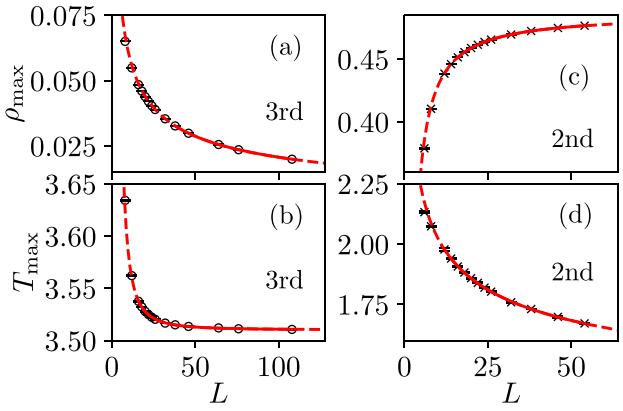

FIG. 13. Behavior of the peak densities of the third and the second largest CMRJ clusters as a function of system size for $\phi = 0.5$. The solid red lines are power-law fits according to Eqs. (25) and (26), respectively. The dashed red lines are extrapolations of the fits. Panels (a) and (b) show the behavior of the peak of the third-largest cluster, and panels (c) and (d) show the same relation for the second-largest cluster.

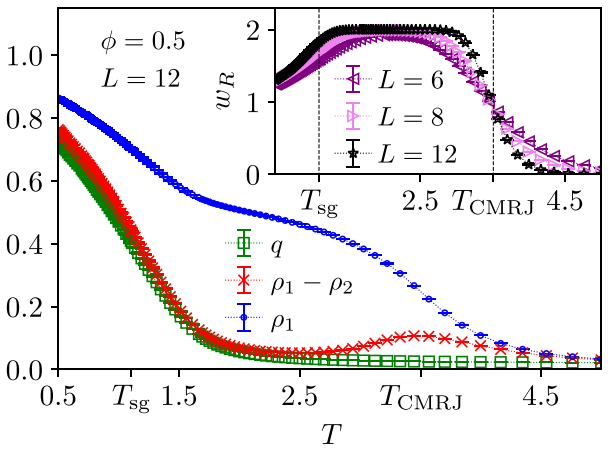

FIG. 14. Relation between the overlap and the density difference of the two largest CMRJ clusters for $\phi = 0.5$ and system size $L = 12$. The inset shows the number of wrapping CMRJ clusters for three different system sizes.

second-largest cluster asymptotically contains nearly half of the spin sites, since $c_{\rho_2} = 0.48582(9)$, with $a_{\rho_2} = -0.709(8)$ and $b_{\rho_2} = 1.092(5)$ for $L_{\rm min} = 16$ and $Q_{\rm fit} = 0.80$.

Figure 14 demonstrates that there is a direct relation between the density difference of the two largest clusters and the overlap. The increase of this quantity below the spin-glass transition signals the onset of spin-glass order and indicates the symmetry-broken phase [29,30]. The inset of Fig. 14 shows the number of wrapping CMRJ clusters for three system sizes. At the CMRJ percolation transition, $T_{\rm CMRJ}$, two wrapping clusters emerge. Below the spin-glass transition, $T_{\rm sg}$, the number of wrapping clusters falls below two.

Notably, the stiffness of the vector spins $\tilde{s}_{\boldsymbol{x}}$ increases with the temperature decreasing from $T_{\rm CMRJ}$ to $T_{\rm sg}$. To demonstrate this, consider the Hamiltonian $\widehat{H}_J^{(2)}$ of Eq. (7), which maintains both a global spin-reversal symmetry $s_{\boldsymbol{x}} \to -s_{\boldsymbol{x}}\ \forall\, \boldsymbol{x}$ and a vector-spin reversal symmetry $\tilde{s}_{\boldsymbol{x}} \to -\tilde{s}_{\boldsymbol{x}}\ \forall\, \boldsymbol{x}$. Interestingly, the latter symmetry breaks at $T_{\rm fr} = 2.045(23)$ when considering dynamics that preserve the site-wise overlap between two replicas, $s_{\boldsymbol{x}}^{(1)} s_{\boldsymbol{x}}^{(2)} = q_{\boldsymbol{x}} = \text{const}\ \forall\, \boldsymbol{x}$. This symmetry breaking suggests that the two-replica Hamiltonian $\widehat{H}_J^{(2)}$ exhibits a form of glassiness even before entering the conventional spin-glass phase. Appendix C provides a more detailed discussion of this conserved-overlap transition.

VII. DISCUSSION

In the present work, we provided an extensive analysis of the relationship between cluster percolation and thermal ordering in the three-dimensional $\pm J$ random-bond Ising model. To develop a comprehensive understanding, both single-replica clusters, such as Ising and FKCK variants, and two-replica clusters, such as the Houdayer and CMRJ definitions, were studied. The latter two cluster types are particularly useful because they are sensitive to the behavior of the overlap, which is the order parameter of the spin-glass transition. The findings indicate that for all studied fractions of antiferromagnetic bonds $0 \leqslant \phi \leqslant 0.5$, there are two giant percolating Houdayer clusters of equal density at high temperatures. These two clusters develop a density difference at the phase transition such that the average overlap becomes nonzero. At ferromagnetic phase transitions, the surface of Houdayer clusters becomes critical, implying large fluctuations in this quantity. In contrast, at the spin-glass transition, there is no singular behavior in the surface of Houdayer clusters.

In the case of CMRJ clusters, the occupation probability decreases with increasing temperatures. As a consequence, only small clusters exist at high temperatures, while at low temperatures, such clusters are almost identical to Houdayer clusters. In the pure ferromagnet, when $\phi = 0$, the CMRJ percolation transition maps onto the ferromagnetic phase transition and shares the same critical behavior. For $\phi > 0$, the CMRJ percolation transition takes place at a higher temperature than either the ferromagnetic or the spin-glass transition and belongs to the random percolation universality class. Geometrically, CMRJ clusters are subregions of Houdayer clusters. In agreement with this, below the percolation transition, there are two large CMRJ clusters of equal density that span the whole system, such that the number of wrapping clusters is two. At the ordering transition, the second-largest cluster reaches its peak size before shrinking, causing the number of wrapping clusters to drop below two. With increasing system size, the locations of these peaks of the second-largest clusters shift to lower temperatures and converge to the (ferromagnetic or spin-glass) ordering transitions, while the peak positions of the third-largest clusters asymptotically approach the corresponding percolation transitions as their density approaches zero.

The density difference between the two largest clusters qualitatively captures the behavior of the overlap. For the Ising ferromagnet, the magnetization, the density difference of the two largest clusters, and the square root of the overlap all coincide in the ordered phase, and hence encapsulate the same scaling behavior. For the disordered ferromagnet, the general correspondence of these quantities is retained, but it is no longer quantitatively accurate. In contrast, for the spin glass, the magnetization is no longer meaningful, and the density difference of the first and second clusters now describes to the overlap itself (instead of its square root), and hence to the order parameter of this transition. This connection allows the spin-glass transition to be identified as an imbalance between the two largest CMRJ clusters. However, there is no direct equivalence between the overlap correlation function and the connectivity function of the CMRJ clusters [29,30]. The main difficulty in identifying clusters that exhibit this property arises from the presence of frustration [21].

Beyond their physical significance, clusters are also used to construct powerful nonlocal Monte Carlo updates [10]. Cluster-based algorithms using Houdayer or CMRJ clusters have proven effective in two-dimensional spin glasses [27,31], significantly accelerating equilibration in Monte Carlo simulations at low temperatures. In three dimensions, however, the same algorithms provide only a modest speedup. This is because the clusters percolate at temperatures higher than the spin-glass transition, implying that the constructed structures are already relatively stiff near the transition. This stiffness of the system is further demonstrated by the conserved-overlap transition, which is described in more detail in Appendix C.

Therefore, to develop better algorithms, it may be useful to identify other types of clusters or nonlocal structures [80–82], for instance, by employing machine learning [83,84] or other simulation techniques [85,86]. Additionally, it may be useful to consider clusters that incorporate more than two replicas [20,23]. Some consequences of this idea are explored in Appendix D.

ACKNOWLEDGMENTS

M.W. is grateful to S. Boettcher for providing an ideal environment and funding for a sabbatical stay at Emory University, where this work was completed.

DATA AVAILABILITY

The data that support the findings of this article are not publicly available upon publication because it is not technically feasible and/or the cost of preparing, depositing, and hosting the data would be prohibitive within the terms of this research project. The data are available from the authors upon reasonable request.

APPENDIX A: CORRELATIONS AND CONNECTIVITY IN CMRJ CLUSTERS

We intend to show that for the case of the pure Ising ferromagnet CMRJ clusters exhibit a relation between connectivity and correlations that is identical to that observed for FKCK clusters. To this end, note that

$$\begin{aligned}\langle \tilde{s}_{\boldsymbol{x}}\tilde{s}_{\boldsymbol{y}}\rangle_{S_2} &= \sum_{\boldsymbol{S}^{(1)},\boldsymbol{S}^{(2)}} \left(s_{\boldsymbol{x}}^{(1)}s_{\boldsymbol{y}}^{(1)} + s_{\boldsymbol{x}}^{(2)}s_{\boldsymbol{y}}^{(2)}\right) P_{S_2}(\boldsymbol{S}^{(1)},\boldsymbol{S}^{(2)}) \\ &= 2\sum_{\boldsymbol{S}} s_{\boldsymbol{x}}s_{\boldsymbol{y}}P_S(\boldsymbol{S}) = 2\langle s_{\boldsymbol{x}}s_{\boldsymbol{y}}\rangle_S, \end{aligned} \tag{A1}$$

where

$$P_S(\boldsymbol{S}) = \frac{1}{Z}\exp\left(\sum_{\langle \boldsymbol{x},\boldsymbol{y}\rangle} s_{\boldsymbol{x}}s_{\boldsymbol{y}}/T\right),$$

and

$$P_{S_2}(\boldsymbol{S}^{(1)},\boldsymbol{S}^{(2)}) = \frac{1}{Z^2}\exp\left(\sum_{\langle \boldsymbol{x},\boldsymbol{y}\rangle} \tilde{s}_{\boldsymbol{x}}\tilde{s}_{\boldsymbol{y}}/T\right).$$

Thus, according to Eq. (A1), the ferromagnetic phase transition described by the single-replica spins $s_{\boldsymbol{x}}$ maps onto the ferromagnetic phase transition of the vector spins $\tilde{s}_{\boldsymbol{x}}$.

Now consider two lattice sites $\boldsymbol{x}$ and $\boldsymbol{y}$. If the corresponding spins belong to the same CMRJ cluster, then $\tilde{s}_{\boldsymbol{x}}\tilde{s}_{\boldsymbol{y}} = 2$. If they belong to different CMRJ clusters, $\tilde{s}_{\boldsymbol{x}}\tilde{s}_{\boldsymbol{y}}$ takes on a value in $\{-2, 0, 2\}$, where, due to spin-flip symmetry, the cases ± 2 occur with equal probabilities. From the perspective of a Monte Carlo Markov chain based on CMRJ clusters, it is clear that each CMRJ cluster can be flipped at random without violating detailed balance [20]. Flipping a CMRJ cluster corresponds to reversing the sign of all vector spins in the cluster, $\tilde{s}_{\boldsymbol{x}} \to -\tilde{s}_{\boldsymbol{x}}\ \forall\ \boldsymbol{x}$ within the cluster. Thus, on average, the product $\tilde{s}_{\boldsymbol{x}}\tilde{s}_{\boldsymbol{y}}$ equals 2 if both spins belong to the same cluster and 0 if they belong to different clusters. From this observation, it follows that

$$\langle \tilde{s}_{\boldsymbol{x}}\tilde{s}_{\boldsymbol{y}}\rangle_{S_2} = 2\,\mathrm{Prob}(\boldsymbol{x} \text{ and } \boldsymbol{y} \text{ are connected}) \tag{A2}$$

after averaging over all spin configurations and all configurations of occupied bonds [5]. Combining this result with Eq. (A1) shows that the connectivity function of CMRJ clusters is identical to the spin–spin correlation function of a single ferromagnet.

APPENDIX B: EXTRAPOLATION ANSATZ FOR SCALING CORRECTIONS

Consider the power-law scaling of an observable O at the critical point, which follows the general form [46,87]

$$\begin{aligned} O(L) &= c_0L^{\theta_0} + c_1L^{\theta_1} + c_2L^{\theta_2} + \cdots \\ &= L^{\theta_0}(c_0 + c_1L^{\tilde{\theta}_1} + c_2L^{\tilde{\theta}_2} + \cdots), \end{aligned} \tag{B1}$$

where we assume that $\theta_i > \theta_{i+1}$ with $i = 0, 1, 2, 3, \ldots$, and $\tilde{\theta}_j = \theta_j - \theta_0$, such that $0 > \tilde{\theta}_j > \tilde{\theta}_{j+1}$ with $j = 1, 2, 3, \ldots$. The terms proportional to L^{θ_i} with $i \geqslant 1$ are scaling corrections that become weaker in comparison to the leading order behavior for large system sizes because $L^{\theta_i}/L^{\theta_0} = L^{\tilde{\theta}_i} \to 0$ for $L \to \infty$. By taking the logarithm of Eq. (B1), we get

$$\ln(O) = \theta_0 \ln(L) + \ln(c_0 + c_1L^{\tilde{\theta}_1} + c_2L^{\tilde{\theta}_2} + \cdots).$$

By substitution of $y_o = \ln(O)$ and $x = \ln(L)$ one obtains

$$\begin{aligned} y_o &= \theta_0 x + \ln(h(x)) \text{ where} \\ h(x) &= c_0 + c_1e^{\tilde{\theta}_1 x} + c_2e^{\tilde{\theta}_2 x} + \cdots. \end{aligned} \tag{B2}$$

Taking the derivative with respect to x gives

$$\theta_{\mathrm{eff}}(x) := \frac{\mathrm{d}y_o}{\mathrm{d}x} = \theta_0 + \frac{h'(x)}{h(x)}. \tag{B3}$$

Because $\lim_{x\to\infty}\frac{\mathrm{d}y_o}{\mathrm{d}x} = \theta_0$ it follows that $h'(x)/h(x) \to 0$. If one only considers first-order scaling corrections $h_1(x) = c_0 + c_1e^{\tilde{\theta}_1 x}$, the correction term becomes

$$\frac{h_1'(x)}{h_1(x)} = \frac{\tilde{\theta}_1}{\frac{c_0}{c_1}e^{-\tilde{\theta}_1 x} + 1}. \tag{B4}$$

Rewriting this as a function of L leads to

$$\frac{\tilde{\theta}_1}{\frac{c_0}{c_1}L^{-\tilde{\theta}_1} + 1}, \tag{B5}$$

and thus $\theta_{\mathrm{eff}} \sim \theta_0 + cL^{\tilde{\theta}_1}$ [87]. To numerically obtain the effective exponents, it is possible to fit a simple power law $f(L) = aL^b$ to local regions of the data, where a and $b = \theta_{\mathrm{eff}}$ are fitting parameters. We denote such a local region that extends from $L_{\min}$ to $L_{\max}$ and includes a fixed number of system sizes, $W = |(L_{\min}, \ldots, L_{\max})|$, as a fit window. The system sizes L_k which are included in the fit windows originate from a logarithmic sequence $x_{k+1} = 2^{1/z}x_k$ where $k = 1, 2, 3, 4, \ldots$. To be more precise, L_k are the rounded values of x_k to the nearest even integer.

Figure 15 illustrates the procedure for the average cluster size of the CMRJ clusters at the critical temperature of the ferromagnetic phase transition. The plot demonstrates how

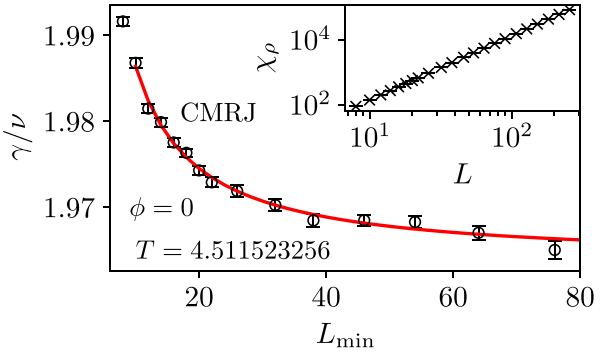

FIG. 15. The main plot shows the dependency of the exponent γ/ν on the fit window for the average cluster size of the CMRJ clusters in the pure Ising ferromagnet ($\phi = 0$). The red line is a fit of type $f(L_{\min}) = a_\theta + b_\theta/(c_\theta\, L_{\min}^{-b_\theta} + 1)$ in accordance with Eq. (B5), where $L_{\min}$ is the smallest system size of each fit window and $a_\theta = \gamma/\nu$ as well as $b_\theta < 0$ and c_θ are fitting parameters. The result is $\gamma/\nu = 1.9638(18)$ where the error bar is computed by bootstrapping as it is described in Ref. [76]. The inset shows the scaling of the average cluster size at $T = 4.511\,523\,256$.

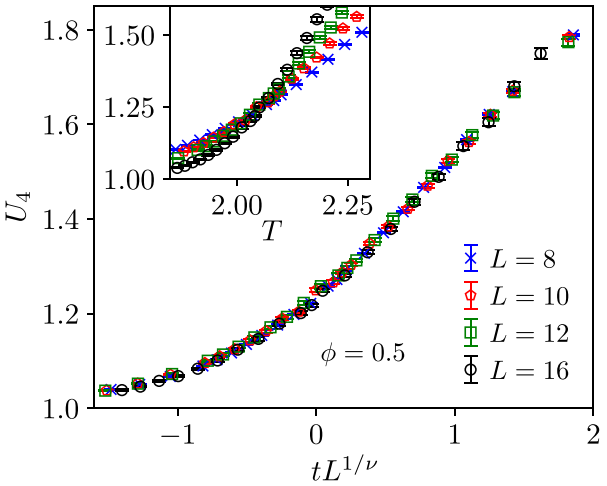

FIG. 16. Data collapse of the U_4 parameter defined in Eq. (C3). The inset shows the original data. The crossing of curves around $T_{\rm fr} = 2.045(23)$ is clearly visible. The fraction of antiferromagnetic bonds is $\phi = 0.5$.

the critical exponent γ/ν is approached by a power law as a function of $L_{\min}$. The system sizes range from $L = 8$ to $L = 256$ and originate from a logarithmic sequence of sizes with $z = 4$. The size of the fit window is $W = 8$. A similar power-law extrapolation was also performed in Ref. [88].

The extrapolation method is applied only for the pure ferromagnet with $\phi = 0$. The corresponding three values of γ/ν, describing the singular behavior of the magnetic susceptibility and the average cluster size of the FKCK and CMRJ clusters, are listed in Table I. For $\phi > 0$, the error due to corrections to scaling has been visually estimated from the convergence behavior of γ/ν as a function of $L_{\min}$, i.e., without applying a power-law extrapolation.

APPENDIX C: THE CONSERVED OVERLAP TRANSITION

Here we show that the two-replica Hamiltonian $\widehat{H}_J^{(2)}$, as defined in Eq. (7), undergoes a phase transition at a higher temperature than the spin-glass transition under a specific dynamical evolution. To explore this, assume that two replicas, $\boldsymbol{S}^{(1)}$ and $\boldsymbol{S}^{(2)}$, are in equilibrium with respect to the Gibbs–Boltzmann distribution for a given realization of disorder $\boldsymbol{J}$. At some point in the Monte Carlo process, say at Monte Carlo time step $t_{\rm fr}$, the relative orientation of the spin components is frozen, which means that $s_{\boldsymbol{x}}^{(1)}(t_{\rm fr})s_{\boldsymbol{x}}^{(2)}(t_{\rm fr}) = q_{\boldsymbol{x}}(t_{\rm fr}) = \text{const}$ from that time onward. This freezing procedure generates the subsidiary Hamiltonian

$$\widehat{H}_J^{(\rm fr)} = -\sum_{\langle \boldsymbol{x},\boldsymbol{y}\rangle} J_{\boldsymbol{xy}}^{(\rm fr)} \tilde{v}_{\boldsymbol{x}} \tilde{v}_{\boldsymbol{y}}, \tag{C1}$$

where

$$\tilde{v}_{\boldsymbol{x}} = \frac{\pm\tilde{s}_{\boldsymbol{x}}(t_{\rm fr})}{\sqrt{2}} = \frac{\pm 1}{\sqrt{2}} \begin{pmatrix} s_{\boldsymbol{x}}^{(1)}(t_{\rm fr}) \\ s_{\boldsymbol{x}}^{(2)}(t_{\rm fr}) \end{pmatrix},$$

and $J_{\boldsymbol{xy}}^{(\rm fr)} = 2J_{\boldsymbol{xy}}$. The product $\tilde{v}_{\boldsymbol{x}}\tilde{v}_{\boldsymbol{y}} = \pm[s_{\boldsymbol{x}}^{(1)}(t_{\rm fr})s_{\boldsymbol{y}}^{(1)}(t_{\rm fr}) + s_{\boldsymbol{x}}^{(2)}(t_{\rm fr})s_{\boldsymbol{y}}^{(2)}(t_{\rm fr})]/2$ can take values ± 1 or 0. After freezing, the system evolves only within the subspace of states where the site-wise overlap remains constant. To achieve this, single-spin flip dynamics for the vector spins, i.e., $\tilde{v}_{\boldsymbol{x}} \to \pm\tilde{v}_{\boldsymbol{x}}$, is implemented alongside CMRJ cluster updates [27], which also preserve the overlap [20].

The order parameter of the conserved-overlap transition is defined as $q_{\rm fr} := [\langle|\widehat{q}_{\rm fr}|\rangle_V]_J$ with

$$\widehat{q}_{\rm fr} = \frac{1}{N}\sum_{\boldsymbol{x}} \tilde{v}_{\boldsymbol{x}}^{(1)}\tilde{v}_{\boldsymbol{x}}^{(2)}. \tag{C2}$$

Here $\tilde{v}_{\boldsymbol{x}}^{(1)}$ and $\tilde{v}_{\boldsymbol{x}}^{(2)}$ belong to two replicas of the system, i.e., $\tilde{v}_{\boldsymbol{x}}^{(1)} \in \tilde{\boldsymbol{V}}^{(1)}$ and $\tilde{v}_{\boldsymbol{x}}^{(2)} \in \boldsymbol{V}^{(2)}$. These replicas are generated by making two identical copies of the vector spins at $t_{\rm fr}$ and then evolving the copies independently in time. This de-correlation of the two replicas requires most of the simulation time. Furthermore, for the order parameter to function correctly, the replicas must be properly aligned. At high temperatures, two giant Houdayer clusters of equal density contain most of the spin sites. Thus, if the replicas $\boldsymbol{V}^{(1)}$ and $\boldsymbol{V}^{(2)}$ are misaligned, $\widehat{q}_{\rm fr}$ can vanish even below the conserved-overlap transition, as long as the Houdayer clusters have equal density. To avoid this, the observable is computed once, yielding the value $\widehat{q}_{\rm fr}^{(a)}$. Next, the largest Houdayer cluster in replica $\boldsymbol{V}^{(2)}$ is flipped and the observable is recomputed as $\widehat{q}_{\rm fr}^{(b)}$. The final estimate is then given by $\widehat{q}_{\rm fr} = \max(|\widehat{q}_{\rm fr}^{(a)}|, |\widehat{q}_{\rm fr}^{(b)}|)$. Flipping a Houdayer cluster means that all vector spins inside the cluster are reversed in sign, $\tilde{v}_{\boldsymbol{x}} \to -\tilde{v}_{\boldsymbol{x}}$. This is a zero-energy transformation because $\tilde{v}_{\boldsymbol{x}}\tilde{v}_{\boldsymbol{y}} = 0$ at the cluster surface, where $\boldsymbol{x}$ is a lattice site inside the cluster and $\boldsymbol{y}$ is a lattice site outside the cluster.

We investigate the conserved-overlap transition with the fraction of antiferromagnetic bonds set to $\phi = 0.5$. To analyze the critical behavior of the transition, the order parameter and its higher moments are studied. Figure 16 shows the dimensionless quantity [89,90]

$$U_4 = \frac{\left[\langle \widehat{q}_{\rm fr}^4\rangle_V\right]_J}{\left[\langle \widehat{q}_{\rm fr}^2\rangle_V\right]_J^2} \tag{C3}$$

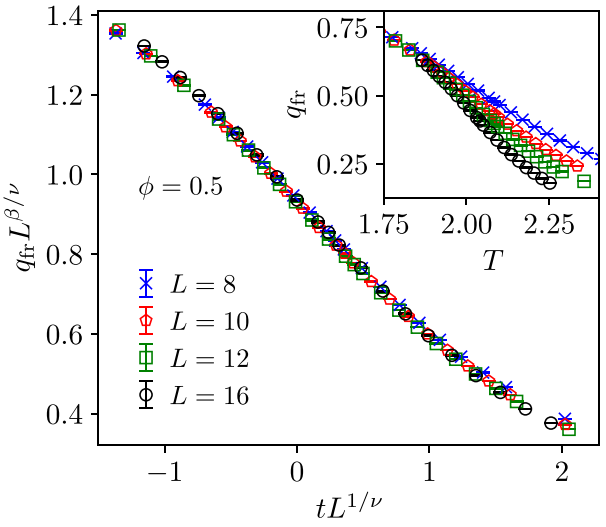

FIG. 17. Data collapse of the conserved-overlap order parameter. The inset shows the original data. The fraction of antiferromagnetic bonds is $\phi = 0.5$.

TABLE IV. Critical quantities of some multiple replica FKCK percolation transitions for three different fractions of antiferromagnetic bonds. K denotes to the number of replicas. The results were obtained by finite-size scaling as described in Sec. III.

		$\phi = 0$	
K	$T_{\rm c}$	ν	γ/ν
1	4.511522(19)	0.630(4)	1.9630(21)
2	2.80981(4)	0.876(7)	2.0454(25)
3	2.006571(29)	0.873(5)	2.048(4)
4	1.63019(4)	0.877(5)	2.043(4)
		$\phi = 0.125$	
K	$T_{\rm c}$	ν	γ/ν
1	4.02079(10)	0.873(4)	2.0451(24)
2	2.39619(18)	0.874(8)	2.043(4)
		$\phi = 0.5$	
K	$T_{\rm c}$	ν	γ/ν
1	3.93410(7)	0.873(4)	2.045(3)
2	1.7315(7)	0.882(9)	2.040(10)

as a function of temperature. The crossing point of the data curves for different system sizes indicates the location of the phase transition. By performing a data collapse according to Eq. (18), the critical temperature is obtained as $T_{\rm fr} = 2.045(23)$ and the exponent as $\nu = 1.00(8)$. The relatively high transition temperature can be attributed to the fact that the couplings of the Hamiltonian in Eq. (C1) are twice as strong as the original couplings. Figure 17 shows a data collapse of the order parameter using Eq. (16), yielding the exponent $\beta/\nu = 0.28(6)$. Additionally, the exponent $\gamma/\nu = 2.33(10)$ is determined by performing a fit according to Eq. (17) with system sizes ranging from $L_{\rm min} = 8$ to $L = 16$. The critical exponents are similar to those found for the phase transition between the ferromagnetic and spin-glass phases in the three-dimensional $\pm J$ random-bond Ising model [44].

In general, it is difficult to obtain precise results for this transition, as long simulation times are required to decorrelate the replicas $\boldsymbol{V}^{(1)}$ and $\boldsymbol{V}^{(2)}$ after freezing at time step $t_{\rm fr}$. Each Monte Carlo time step after freezing consists of one CMRJ cluster update and one sweep of single vector-spin flips. The system sizes used range from $L = 8$ to $L = 16$. For $L = 8$, up to 181 261 disorder samples were generated with a de-correlation time of $t_{\rm d} = 120\,000$, whereas for $L = 16$, up to 30 875 samples were generated with $t_{\rm d} = 1\,600\,000$.

APPENDIX D: MULTIPLE REPLICA FKCK PERCOLATION

In Sec. II, we introduced Houdayer and CMRJ clusters, which are based on two replicas. Independently, Newman and Stein proposed a method for defining clusters using two replicas [29,57], which can be directly extended to more than two replicas [20]. The bond-occupation probability for these clusters with K replicas is defined as

$$p_{xy}^{(K)} = \begin{cases} (1 - e^{-2/T})^K & \text{if } J_{xy}\tilde{s}_x\tilde{s}_y = K \\ 0 & \text{else,} \end{cases} \tag{D1}$$

where $\tilde{s}_x\tilde{s}_y = \sum_{k=1}^{K} s_x^{(k)} s_y^{(k)}$. As a consequence, bonds can only be occupied if they are satisfied in all K replicas simultaneously, i.e., $J_{xy}s_x^{(k)}s_y^{(k)} = 1$ for all $k = 1, 2, \ldots, K$. When $K = 1$, the definition reduces to that of the standard FKCK clusters given in Eq. (10).

Multiple-replica FKCK clusters were originally introduced as a mathematical tool to prove broken symmetry in spin glasses [29,57]. The appearance of a unique infinite multiple-replica FKCK cluster with $K > 1$ implies the existence of broken symmetry in spin glasses [29,30,57]. However, their physical interpretation remains unclear.

The percolation transitions of these clusters were analyzed for different values of K and $\phi \in \{0, 0.125, 0.5\}$. Except for the FKCK clusters in the pure Ising ferromagnet, all considered transitions belong to the random-percolation universality class, as summarized in Table IV. For $\phi = 0$ and $K > 1$, the percolation temperature $T_{\rm c}$ can be roughly estimated from the bond-percolation threshold of the cubic lattice [50], $p_{\rm th} = 0.248\,811\,82(10)$, through the relation $p_{\rm th} \approx (1 - e^{-2/T_{\rm c}})^K$.

For $\phi = 0.125$ and $K = 2$, the clusters percolate at a temperature below the ferromagnetic transition, while for $\phi = 0.5$ they percolate above the spin-glass temperature. For the considered numbers of replicas, there appears to be no direct connection between the percolation of multiple-replica FKCK clusters and ordering transitions. It would be interesting, however, to investigate whether a choice of $K > 2$ for the disordered cases leads to situations where the percolation transition (nearly or exactly) coincides with the ordering transition.

APPENDIX E: SIMULATION DETAILS

In our simulations, three types of Monte Carlo updates are employed: single-spin flip updates, Swendsen–Wang cluster updates, and CMRJ cluster updates. The first two are described, for example, in Ref. [91]. The CMRJ cluster updates work as follows. First, the clusters are constructed accord-

ing to the probabilistic rule given in Eq. (12). Then, each cluster is flipped with probability 0.5. While CMRJ cluster updates satisfy detailed balance with respect to the two-replica Gibbs–Boltzmann distribution, they are not ergodic due to the conservation of overlap. Therefore, they need to be augmented by ergodic updates such as single-spin flips or Swendsen–Wang cluster updates. In addition to these single-replica moves, parallel tempering is implemented with a chain of system copies simulated at different temperatures [91]. For the latter, we used between 20 and 40 temperatures, in general spaced uniformly in inverse temperature. To ensure sufficient acceptance rates for the swap moves of at least 10%, additional temperature points were inserted when required.

Depending on the fraction of antiferromagnetic bonds, different combinations of Monte Carlo updates are used. For $\phi = 0$, the Swendsen–Wang algorithm is employed exclusively, such that each Monte Carlo time step consists of a single Swendsen–Wang cluster update. As a criterion for equilibration, the Monte Carlo process is initialized from both a ground-state configuration and a high-temperature configuration, and the simulation is continued until both processes oscillate around the same average value. Measurements are started after equilibration. To ensure that the measurements are approximately uncorrelated, one sample is extracted only after at least twice the integrated autocorrelation time [63]. The system size typically ranges from $L = 16$ to $L = 128$. For $L = 16$, for example, 500 000 samples were generated, while for $L = 128$ about 26 000 samples were obtained to analyze the ferromagnetic phase transition. Note that precisely at the critical temperature a larger range of system sizes, from $L = 8$ up to $L = 256$, was simulated with longer run times.

For $\phi > 0$, Swendsen–Wang cluster updates combined with parallel tempering were used to study the FKCK percolation transition, which occurs at relatively high temperatures. At lower temperatures, one Monte Carlo time step consists of a sweep of single-spin flips, a CMRJ cluster update, and a parallel tempering move. The relaxation time is estimated from the time evolution of the link overlap, starting from random initial spin configurations. The system is considered to be in equilibrium when the link overlap reaches a stationary value in time, averaged over disorder, see Ref. [92]. For the data analysis, at least 1000 disorder samples were generated for all system sizes and the lowest considered temperatures. The system size typically ranges from $L = 16$ to $L = 90$ for studying the CMRJ percolation transition. For the data shown in Fig. 6, for instance, the number of disorder samples is 20 597 for $L = 32$ and 2886 for $L = 108$.

[1] M. E. Fisher, The theory of condensation and the critical point, Phys. Phys. Fiz. **3**, 255 (1967).

[2] E. Luijten, Introduction to cluster Monte Carlo algorithms, Lect. Notes Phys. **703**, 13 (2006).

[3] A. Coniglio and A. Fierro, Correlated percolation, in *Complex Media and Percolation Theory*, edited by M. Sahimi and A. G. Hunt (Springer, New York, 2021), pp. 61–88.

[4] R. A. L. Almeida, Critical percolation in the ordering kinetics of twisted nematic phases, Phys. Rev. Lett. **131**, 268101 (2023).

[5] G. Grimmett, *The Random-Cluster Model* (Springer, Berlin, 2004).

[6] C. M. Fortuin and P. W. Kasteleyn, On the random-cluster model: I. Introduction and relation to other models, Physica **57**, 536 (1972).

[7] A. Coniglio and W. Klein, Clusters and Ising critical droplets: a renormalisation group approach, J. Phys. A: Math. Gen. **13**, 2775 (1980).

[8] R. H. Swendsen and J. S. Wang, Nonuniversal critical dynamics in Monte Carlo simulations, Phys. Rev. Lett. **58**, 86 (1987).

[9] U. Wolff, Collective Monte Carlo updating for spin systems, Phys. Rev. Lett. **62**, 361 (1989).

[10] W. Janke, Nonlocal Monte Carlo algorithms for statistical physics applications, Math. Comp. Simul. **47**, 329 (1998).

[11] U. Wolff, Comparison between cluster Monte Carlo algorithms in the Ising model, Phys. Lett. B **228**, 379 (1989).

[12] K. Binder and A. P. Young, Spin glasses: Experimental facts, theoretical concepts, and open questions, Rev. Mod. Phys. **58**, 801 (1986).

[13] D. L. Stein and C. M. Newman, *Spin Glasses and Complexity* (Princeton University Press, Princeton, 2013).

[14] H. Nishimori, *Statistical Physics of Spin Glasses and Information Processing: An Introduction* (Oxford University Press, Oxford, 2001).

[15] *Spin Glass Theory and Far Beyond*, edited by P. Charbonneau, E. Marinari, M. Mézard, G. Parisi, F. Ricci-Tersenghi, G. Sicuro, and F. Zamponi (World Scientific, Singapore, 2023).

[16] L. de Arcangelis, A. Coniglio, and F. Peruggi, Percolation transition in spin glasses, Europhys. Lett. **14**, 515 (1991).

[17] A. Coniglio, F. di Liberto, G. Monroy, and F. Peruggi, Cluster approach to spin glasses and the frustrated-percolation problem, Phys. Rev. B **44**, 12605 (1991).

[18] E. De Santis and A. Gandolfi, Bond percolation in frustrated systems, Ann. Probab. **27**, 1781 (1999).

[19] H. Fajen, A. K. Hartmann, and A. P. Young, Percolation of Fortuin-Kasteleyn clusters for the random-bond Ising model, Phys. Rev. E **102**, 012131 (2020).

[20] L. Münster and M. Weigel, Cluster percolation in the two-dimensional Ising spin glass, Phys. Rev. E **107**, 054103 (2023).

[21] V. Cataudella, G. Franzese, M. Nicodemi, A. Scala, and A. Coniglio, Critical clusters and efficient dynamics for frustrated spin models, Phys. Rev. Lett. **72**, 1541 (1994).

[22] G. A. Miranda, M. Zheng, P. Charbonneau, A. Coniglio, L. F. Cugliandolo, and M. Tarzia, Percolation and criticality of systems with competing interactions on Bethe lattices: Limitations and potential strengths of cluster schemes, arXiv:2510.02961.

[23] R. H. Swendsen and J.-S. Wang, Replica Monte Carlo simulation of spin-glasses, Phys. Rev. Lett. **57**, 2607 (1986).

[24] M. Akritidis, N. G. Fytas, and M. Weigel, Geometric clusters in the overlap of the Ising model, Phys. Rev. E **108**, 044145 (2023).

[25] L. Münster and M. Weigel, Spin glasses and percolation, Front. Phys. **12**, 1448175 (2024).

[26] L. Chayes, J. Machta, and O. Redner, Graphical representations for Ising systems in external fields, J. Stat. Phys. **93**, 17 (1998).

[27] T. Jörg, Cluster Monte Carlo algorithms for diluted spin glasses, Prog. Theor. Phys. Suppl. **157**, 349 (2005).

[28] D. Sherrington and S. Kirkpatrick, Solvable model of a spin-glass, Phys. Rev. Lett. **35**, 1792 (1975).
[29] J. Machta, C. Newman, and D. Stein, The percolation signature of the spin glass transition, J. Stat. Phys. **130**, 113 (2007).
[30] J. Machta, C. M. Newman, and D. L. Stein, A percolation-theoretic approach to spin glass phase transitions, in *Spin Glasses: Statics and Dynamics*, Progress in Probability (Birkhäuser, Basel, 2009), pp. 205–223.
[31] J. Houdayer, A cluster Monte Carlo algorithm for 2-dimensional spin glasses, Eur. Phys. J. B **22**, 479 (2001).
[32] J.-S. Wang and R. H. Swendsen, Low-temperature properties of the $\pm J$ Ising spin glass in two dimensions, Phys. Rev. B **38**, 4840 (1988).
[33] O. Redner, J. Machta, and L. F. Chayes, Graphical representations and cluster algorithms for critical points with fields, Phys. Rev. E **58**, 2749 (1998).
[34] J. Machta, M. E. J. Newman, and L. B. Chayes, Replica-exchange algorithm and results for the three-dimensional random field Ising model, Phys. Rev. E **62**, 8782 (2000).
[35] J.-S. Wang and R. H. Swendsen, Replica Monte Carlo simulation (revisited), Prog. Theor. Phys. Suppl. **157**, 317 (2005).
[36] T. Jörg, Critical behavior of the three-dimensional bond-diluted Ising spin glass: Finite-size scaling functions and universality, Phys. Rev. B **73**, 224431 (2006).
[37] M. Hasenbusch, Thermodynamic Casimir forces between a sphere and a plate: Monte Carlo simulation of a spin model, Phys. Rev. E **87**, 022130 (2013).
[38] Z. Zhu, A. J. Ochoa, and H. G. Katzgraber, Efficient cluster algorithm for spin glasses in any space dimension, Phys. Rev. Lett. **115**, 077201 (2015).
[39] M. Hasenbusch, Variance-reduced estimator of the connected two-point function in the presence of a broken $\mathbb{Z}_2$-symmetry, Phys. Rev. E **93**, 032140 (2016).
[40] M. Hasenbusch, F. P. Toldin, A. Pelissetto, and E. Vicari, Critical and multicritical behavior of the $\pm J$ Ising model in two and three dimensions, J. Phys.: Conf. Ser. **145**, 012055 (2009).
[41] M. Hasenbusch, F. P. Toldin, A. Pelissetto, and E. Vicari, Critical behavior of the three-dimensional $\pm J$ Ising model at the paramagnetic-ferromagnetic transition line, Phys. Rev. B **76**, 094402 (2007).
[42] M. Hasenbusch, A. Pelissetto, and E. Vicari, Critical behavior of three-dimensional Ising spin glass models, Phys. Rev. B **78**, 214205 (2008).
[43] M. Hasenbusch, F. P. Toldin, A. Pelissetto, and E. Vicari, Magnetic-glassy multicritical behavior of the three-dimensional $\pm J$ Ising model, Phys. Rev. B **76**, 184202 (2007).
[44] G. Ceccarelli, A. Pelissetto, and E. Vicari, Ferromagnetic-glassy transitions in three-dimensional Ising spin glasses, Phys. Rev. B **84**, 134202 (2011).
[45] C. K. Thomas and H. G. Katzgraber, Sampling the ground-state magnetization of d-dimensional p-body Ising models, Phys. Rev. B **84**, 174404 (2011).
[46] A. M. Ferrenberg, J. Xu, and D. P. Landau, Pushing the limits of Monte Carlo simulations for the three-dimensional Ising model, Phys. Rev. E **97**, 043301 (2018).
[47] H. G. Katzgraber, M. Körner, and A. P. Young, Universality in three-dimensional Ising spin glasses: A Monte Carlo study, Phys. Rev. B **73**, 224432 (2006).
[48] M. Baity-Jesi, R. A. Baños, A. Cruz, L. A. Fernandez, J. M. Gil-Narvion, A. Gordillo-Guerrero, D. Iniguez, A. Maiorano, F. Mantovani, E. Marinari, *et al.*, Critical parameters of the three-dimensional Ising spin glass, Phys. Rev. B **88**, 224416 (2013).
[49] A. K. Hartmann, Ground-state behavior of the three-dimensional $\pm J$ random-bond Ising model, Phys. Rev. B **59**, 3617 (1999).
[50] J. Wang, Z. Zhou, W. Zhang, T. M. Garoni, and Y. Deng, Bond and site percolation in three dimensions, Phys. Rev. E **87**, 052107 (2013).
[51] H. Nishimori, Exact results and critical properties of the Ising model with competing interactions, J. Phys. C: Solid State Phys. **13**, 4071 (1980).
[52] H. Nishimori, Internal energy, specific heat and correlation function of the bond-random Ising model, Prog. Theor. Phys. **66**, 1169 (1981).
[53] C. Yamaguchi, Conjectured exact percolation thresholds of the Fortuin–Kasteleyn cluster for the Ising spin glass model, Phys. A (Amsterdam, Neth.) **392**, 1263 (2013).
[54] C. Yamaguchi, Percolation thresholds of the Fortuin–Kasteleyn cluster for the Edwards-Anderson Ising model on complex networks: Analytical results on the Nishimori line, Prog. Theor. Phys. **124**, 399 (2010).
[55] A. Gandolfi, A remark on gauge symmetries in Ising spin glasses, Probab. Theory Relat. Fields **114**, 419 (1999).
[56] P. H. Lundow and I. A. Campbell, Fortuin-Kasteleyn and damage-spreading transitions in random-bond Ising lattices, Phys. Rev. E **86**, 041121 (2012).
[57] C. M. Newman and D. L. Stein, Short-range spin glasses: Results and speculations, in *Spin Glasses* (Springer, Berlin, 2007), pp. 159–175.
[58] In the graphical representation of Chayes, Machta and Redner the CMRJ clusters are actually denoted as blue clusters. Here, we use the acronym CMRJ for blue clusters [29].
[59] D. Stauffer and A. Aharony, *Introduction to Percolation Theory*, 2nd ed. (Taylor & Francis, London, 1994).
[60] *Complex Media and Percolation Theory*, edited by M. Sahimi and A. G. Hunt (Springer, New York, 2021).
[61] G. Grimmett, *Percolation*, 2nd ed. (Springer, Berlin, 1999).
[62] M. E. J. Newman and R. M. Ziff, Fast Monte Carlo algorithm for site or bond percolation, Phys. Rev. E **64**, 016706 (2001).
[63] W. Janke, Monte Carlo methods in classical statistical physics, in *Computational Many-Particle Physics*, Lectures Notes Physics edited by H. Fehske, R. Schneider, and A. Weiße (Springer, Berlin, 2008), Vol. 739, pp. 79–140.
[64] H. Nishimori and G. Ortiz, Renormalization group and scaling, in *Elements of Phase Transitions and Critical Phenomena* (Oxford University Press, Oxford, 2011), pp. 52–82.
[65] O. Melchert, autoScale.py - A program for automatic finite-size scaling analyses: A user's guide, arXiv:0910.5403.
[66] H. Müller-Krumbhaar, Percolation in a lattice system with particle interaction, Phys. Lett. A **50**, 27 (1974).
[67] The percolation temperature $T_{\rm lcl} = 4.3027(3)$, as well as the critical exponent $\nu = 0.882(5)$, are extracted by performing a data collapse of the number of wrapping Ising clusters, i.e., $w_R(t, L) = \Psi_w(tL^{1/\nu})$, where $t = (T - T_{\rm lcl})/T_{\rm lcl}$ (plot not shown). The exponent is consistent with random percolation.

[68] A. L. Stella and C. Vanderzande, Scaling and fractal dimensions of Ising clusters at the $d = 2$ critical point, Phys. Rev. Lett. **62**, 1067 (1989).
[69] S. Fortunato, Cluster percolation and critical behavior in spin models and $SU(N)$ gauge theories, J. Phys. A: Math. Gen. **36**, 4269 (2003).
[70] A. R. de la Rocha, P. M. C. de Oliveira, and J. J. Arenzon, Domain-size heterogeneity in the Ising model: Geometrical and thermal transitions, Phys. Rev. E **91**, 042113 (2015).
[71] L. Bai and D. Breen, Calculating center of mass in an unbounded 2d environment, J. Graph. Tools **13**, 53 (2008).
[72] M. Weigel, W. Janke, and C.-K. Hu, Random-cluster multihistogram sampling for the q-state Potts model, Phys. Rev. E **65**, 036109 (2002).
[73] M. Suzuki, Solution of Potts model for phase transition, Prog. Theor. Phys. **37**, 770 (1967).
[74] M. Aizenman and B. Simon, A comparison of plane rotor and Ising models, Phys. Lett. A **76**, 281 (1980).
[75] M. Hasenbusch, F. P. Toldin, A. Pelissetto, and E. Vicari, The universality class of 3D site-diluted and bond-diluted Ising systems, J. Stat. Mech. (2007) P02016.
[76] A. P. Young, *Everything You Wanted to Know About Data Analysis and Fitting But Were Afraid to Ask* (Springer, Cham, 2015).
[77] C. M. Newman and D. L. Stein, Local vs global variables for spin glasses, in *Spin Glasses*, edited by E. Bolthausen and A. Bovier (Springer, Berlin, 2007), pp. 145–158.
[78] P. Contucci, Replica equivalence in the Edwards-Anderson model, J. Phys. A: Math. Gen. **36**, 10961 (2003).
[79] A. Bray and M. Moore, Some observations on the mean-field theory of spin glasses, J. Phys. C: Solid State Phys. **13**, 419 (1980).
[80] D. Kandel, R. Ben-Av, and E. Domany, Cluster dynamics for fully frustrated systems, Phys. Rev. Lett. **65**, 941 (1990).
[81] P. D. Coddington and L. Han, Generalized cluster algorithms for frustrated spin models, Phys. Rev. B **50**, 3058 (1994).
[82] V. Cataudella, G. Franzese, M. Nicodemi, A. Scala, and A. Coniglio, Percolation and cluster Monte Carlo dynamics for spin models, Phys. Rev. E **54**, 175 (1996).
[83] J. Liu, Y. Qi, Z. Y. Meng, and L. Fu, Self-learning Monte Carlo method, Phys. Rev. B **95**, 041101(R) (2017).
[84] B. McNaughton, M. V. Milošević, A. Perali, and S. Pilati, Boosting Monte Carlo simulations of spin glasses using autoregressive neural networks, Phys. Rev. E **101**, 053312 (2020).
[85] L. Wang, Exploring cluster Monte Carlo updates with Boltzmann machines, Phys. Rev. E **96**, 051301(R) (2017).
[86] Y. R. Pei and M. Di Ventra, Non-equilibrium criticality and efficient exploration of glassy landscapes with memory dynamics, Phys. A (Amsterdam, Neth.) **591**, 126727 (2022).
[87] A. Aharony and G. Ahlers, Universal ratios among correction-to-scaling amplitudes and effective critical exponents, Phys. Rev. Lett. **44**, 782 (1980).
[88] L. Münster, C. Norrenbrock, A. K. Hartmann, and A. P. Young, Ordering behavior of the two-dimensional Ising spin glass with long-range correlated disorder, Phys. Rev. E **103**, 042117 (2021).
[89] K. Binder, Finite size scaling analysis of Ising model block distribution functions, Z. Phys. B: Condens. Matter **43**, 119 (1981).
[90] K. Binder, Critical properties from Monte Carlo coarse graining and renormalization, Phys. Rev. Lett. **47**, 693 (1981).
[91] M. E. Newman and G. T. Barkema, *Monte Carlo Methods in Statistical Physics* (Oxford University Press, Oxford, 1999).
[92] H. G. Katzgraber, M. Palassini, and A. P. Young, Monte Carlo simulations of spin glasses at low temperatures, Phys. Rev. B **63**, 184422 (2001).